IEEE Access
Multidisciplinary | Rapid Review | Open Access Journal

Received January 26, 2021, accepted February 2, 2021, date of publication February 10, 2021, date of current version February 22, 2021.

Digital Object Identifier 10.1109/ACCESS.2021.3058387

CNN-Based Intelligent Fault-Tolerant Control Design for Turbofan Engines With Actuator Faults

DINGDING CHENG[1,2], LIJUN LIU[1,2], AND ZHEN YU[1]
[1]School of Aerospace Engineering, Xiamen University, Xiamen 361005, China
[2]Shenzhen Research Institute of Xiamen University, Shenzhen 518000, China

Corresponding author: Zhen Yu (yuzhen20@xmu.edu.cn)

This work was supported in part by the National Natural Science Foundation of China under Grant 61304110, in part by the Natural Science Foundation of Fujian under Grant 2020J01052, in part by the Guangdong Natural Science Foundation under Grant 2018A030313124, in part by the Basic Research Program of Science and Technology of Shenzhen under Grant JCYJ20190809163009630, and in part by the Natural Science Foundation of Shanghai under Grant 18ZR1443200.

ABSTRACT In this paper, the problem of fault-tolerant control is investigated for turbofan engines with actuator faults. The controller involvement has repressed the effects of actuator faults on the controlled outputs of turbofan engines, making fault-tolerant control difficult. To solve this problem, the internal gas-path data of turbofan engines is introduced to provide conducive fault information. Besides, the useful property of the convolution neural network (CNN) is explored and utilized in fault-tolerant control. Based on the analysis of actuator faults, by using the Lyapunov stability and L_2-gain like theorems, a novel CNN-based intelligent fault-tolerant control system for turbofan engines is proposed, including a CNN-based fault diagnosis module and a nonlinear fault-tolerant control with corresponding reconfiguration unit. The CNN-based intelligent fault-tolerant control system has the advantages of reducing the accuracy requirements of the mathematical description of turbofan engines. Furthermore, the proposed system can diagnose actuator faults and reduce the adverse effects of actuator faults on turbofan engines. Finally, simulation results are presented to demonstrate the efficiency of the designed method.

INDEX TERMS CNN-based intelligent fault-tolerant control, actuator faults, gas-path data, fault diagnosis, nonlinear fault-tolerant controller, turbofan engines.

I. INTRODUCTION

In the event of actuator faults, the controlled outputs of turbofan engines are with small changes for a short time due to controller engagement [1]. The unappealing phenomenon may lead to the so-called effect of actuator faults, which has serious consequences and even produces catastrophic accidents [2]–[5]. Fault-tolerant control plays a critical role in enhancing the safety and reliability of turbofan engines. The existing fault-tolerant control techniques of turbofan engines are categorized into two classes: passive approach and active approach [6], [7]. The parameters of the passive fault-tolerant control are selected overly conservatively such that the turbofan engines may have a loss of performance in the nominal case [8]. On the contrary, the active fault-tolerant controller can be reconfigured flexibly according to the faults information provided by the diagnosis module to reduce the conservation. Therefore, the research on active fault-tolerant control (AFTC) for turbofan engines has received some attention.

The fault diagnosis of AFTC is to provide all possible information regarding the abnormal functioning of systems. As one of the most important technologies of fault diagnosis, redundancy is to monitor, isolate and estimate system faults by obtaining multiple signals of the same variable. Redundancy is mainly divided into hardware redundancy and analytical redundancy [9]. In hardware redundancy, multiple backup sensors or actuators are used to perform the same task thereby preventing the failure of the system [10], such as dual redundancy [11], triple modular redundancy [12], and modified triple redundancy [13]. Owing to increasing the cost, weight, and physical size, hardware redundancy is often not an option for turbofan engines. In analytical redundancy, filters [12], adaptive observers [14], linear regression-based observers [15] are designed to estimate the operation of components, which are mainly used in the case of sensor faults. To estimate actuator faults, many other fault diagnosis approaches have been proposed for turbofan engines, such

The associate editor coordinating the review of this manuscript and approving it for publication was Feiqi Deng.

as Kalman filter [16]–[21], observer [22], [23], and other related methods [16], [24]–[28]. These approaches detect actuator faults only based on the behaviour of the controlled outputs. However, due to controller engagement, the small change of the controlled outputs makes fault detection difficult. Besides, some of these fault diagnosis approaches are developed as a diagnostic or monitoring tool, rather than an integral part of the fault-tolerant control system for turbofan engines.

The fault-tolerant controller of AFTC is to adjust the system against faults for the stable operation according to the fault information. Some interesting work has been reported on the design of fault-tolerant controllers, such as robust control [29], sliding mode control [30], and other methods [31]. For instance, considering time-varying delay, actuator saturation, and actuator faults, R. Sakthivel *et al.* proposed a nonlinear fault-tolerant controller method to guarantee the finite-time stability of the closed-loop system [31]. For power systems with actuator failures, time-varying delays, and admissible parameter uncertainties, B. Kaviarasan *et al.* designed a fault-tolerant state feedback controller by linear matrix inequality based optimization algorithm to guarantee the robust stochastic stability of the whole system [32]. These controllers require accurate fault information during the design process. Nevertheless, most of the above fault-tolerant controllers assume that a perfect fault diagnosis scheme is available. Without proper consideration of the fault diagnosis parts, combined AFTC systems with these controllers may do not work as expected.

Each part of the integrated AFTC is taken into account in the design to ensure the coordinated operation [33]. Much research in recent years has focused on the integrated AFTC for turbofan engines [34]–[36]. In the work of X. Liu *et al.* [34], a jointly state/fault estimator and a corresponding output feedback controller were constructed to guarantee the input-to-state stability and mitigate fault effects. In the presence of the sensor and actuator faults, Xiao *et al.* [35] designed an adaptive observer and a sliding mode fault-tolerant controller to stabilize aircraft engine systems. Chang *et al.* [36] applied a second-order sliding mode observer to estimate the engine states and sensor faults and then designed an estimated-state feedback controller against the faults for aircraft engines. One feature of the works mentioned above is that the integrated AFTC needs not only the precise mathematical description of turbofan engines but also the reliable observer-based fault-detection residual. However, the accuracy of the mathematical description cannot be guaranteed due to the complex structure of turbofan engines. The residual can magnify or suppress the fault information and not always be effective [1]. Besides, the lack of the self-organizing and self-learning abilities of these methods is rooted in the fact.

Motivated by the above discussion, except for controlled outputs, other operational information of turbofan engines needs to be introduced into fault diagnosis to improve the reliability of AFTC. The design of the AFTC method should also reduce the dependence of the mathematical description of turbofan engines. Furthermore, the AFTC method of turbofan engines is expected to operate in coordination and intelligence with full consideration to each part. To solve the above problems, a CNN-based intelligent fault-tolerant control (CIFTC) method is proposed for turbofan engines against actuator faults. Firstly, besides the controlled outputs, the internal operation data of turbofan engines is used to enrich fault information. Secondly, a CNN-based diagnosis module is designed to detect actuator faults to avoid the adverse effects of the imprecise mathematical description of turbofan engines. Thirdly, we develop an integrated CIFTC system for turbofan engines. The Lyapunov function and L_2-gain like theorems are used for the stability proof of the CIFTC system. Simulation results show that the proposed method is an effective tool for handling fault-tolerant control issues for turbofan engines.

The main contributions of the paper can be summarized as follows.

1) The measurable gas-path data of turbofan engines is introduced into the CIFTC system. Compared with [17]–[23], [34]–[36], more operational data is utilized in fault diagnosis to solve the problem of limited fault information provided by the controlled outputs.
2) The CNN-based diagnosis module is proposed for turbofan engines. The characteristics of CNN is developed for the proposed diagnosis module. The data-based diagnosis method can relax the accuracy requirements of the mathematical description of turbofan engines for the CIFTC system.
3) An integrated CIFTC system is designed for turbofan engines against actuator faults. The system consists of the CNN-based diagnosis module, a nonlinear fault-tolerant controller, and the corresponding reconfiguration unit. Each part of CIFTC is unified in the framework of the nonlinear H_∞ control theory, which can ensure the stability and control performance of the closed-loop system for turbofan engines.

The rest of the paper is organized as follows. In Section II, the modeling of turbofan engines with actuator faults is given. Besides, the objective of CIFTC is formulated. In Section III, the structure of the proposed CIFTC system is presented. In Section IV, the CNN-based fault diagnosis module is developed. In Section V, the design method, theory, and solution of the nonlinear fault-tolerant controllers for turbofan engines are given. Case studies are presented in Section VI. Finally, Section VII draws the conclusion.

Notations: In this paper, $\mathbb{R}$, $\mathbb{R}^n$, and $\mathbb{R}^{n\times m}$ denote the real numbers, the real n-vectors and the real $n\times m$ matrices, respectively. If x denotes a given vector or matrix, then x^T indicates its transpose. The variables with Δ represents the deviation of engine variables from their steady-state values for the specified operation condition. We denote by $diag(a_1, \ldots, a_n)$ a block diagonal matrix with $a_1, \ldots, a_n$ as the diagonal elements. Let $0_{a\times b}$ and 0_a represent the zero

TABLE 1. Classifications and modes of actuator faults for turbofan engines.

Actuator	Fault example	Fault type	Label	Fault mode	$\phi_f^{a,i}$ or $\phi_f^{m,i}$	$\varrho_f^{a,i}$ or $\varrho_f^{m,i}$
Δwf	Zero-drift of sensors	Additive	L_0	wf,a,1	$\phi_f^{a,1}=\phi_f^{a,1,1}$	$\varrho_f^{a,1}\in\left[\overline{\varrho}_f^{a,1,1}\ \ \underline{\varrho}_f^{a,1,1}\right]$
			L_1	wf,a,2	$\phi_f^{a,1}=\phi_f^{a,1,2}$	$\varrho_f^{a,1}\in\left[\overline{\varrho}_f^{a,1,2}\ \ \underline{\varrho}_f^{a,1,2}\right]$
	Degradation of sensitive elements	Multiplicative	L_0	wf,m,1	$\phi_f^{m,1}=\phi_f^{m,1,1}$	$\varrho_f^{m,1}\in\left[\overline{\varrho}_f^{m,1,1}\ \ \underline{\varrho}_f^{m,1,1}\right]$
			L_2	wf,m,2	$\phi_f^{m,1}=\phi_f^{m,1,2}$	$\varrho_f^{m,1}\in\left[\overline{\varrho}_f^{m,1,2}\ \ \underline{\varrho}_f^{m,1,2}\right]$
			L_3	wf,m,3	$\phi_f^{m,1}=\phi_f^{m,1,3}$	$\varrho_f^{m,1}\in\left[\overline{\varrho}_f^{m,1,3}\ \ \underline{\varrho}_f^{m,1,3}\right]$
Δvsv	Valve deviation	Additive	L_0	vsv,a,1	$\phi_f^{a,2}=\phi_f^{a,2,1}$	$\varrho_f^{a,2}\in\left[\overline{\varrho}_f^{a,2,1}\ \ \underline{\varrho}_f^{a,2,1}\right]$
			L_4	vsv,a,2	$\phi_f^{a,2}=\phi_f^{a,2,2}$	$\varrho_f^{a,2}\in\left[\overline{\varrho}_f^{a,2,2}\ \ \underline{\varrho}_f^{a,2,2}\right]$
	Daming stagnation	Multiplicative	L_0	vsv,m,1	$\phi_f^{m,2}=\phi_f^{m,2,1}$	$\varrho_f^{m,2}\in\left[\overline{\varrho}_f^{m,2,1}\ \ \underline{\varrho}_f^{m,2,1}\right]$
			L_5	vsv,m,2	$\phi_f^{m,2}=\phi_f^{m,2,2}$	$\varrho_f^{m,2}\in\left[\overline{\varrho}_f^{m,2,2}\ \ \underline{\varrho}_f^{m,2,2}\right]$

matrices with dimensions $a\times b$ and $a\times a$. Let I_n represent an identity matrix with dimension n.

II. PROBLEM FORMULATION

In this section, the modeling of actuator faults is presented firstly. Then, the polynomial state-space model of turbofan engines is introduced. The objective of CIFTC for turbofan engines with actuator faults is given finally.

A. MODELING OF ACTUATOR FAULTS

Multiple operating loads, long-running, and poor conditions may cause actuator faults of turbofan engines [21], [37]. As shown in Table 1, these unavoidable fault examples of turbofan engines can result in the degradation of actuators. The actuator degradation leads to a mismatch (called fault inputs) between actual inputs and commanded inputs. In the event of actuator faults, the actual input $\Delta u(t)=\left[\Delta wf\ \ \Delta vsv\right]^T\in\mathbb{R}^q$ is composed of commanded control inputs and fault inputs given by

$$\Delta u(t)=\Delta u_c(t)+\Delta u_f(t), \tag{1}$$

where the variables labeled c and f denote the commanded input and the fault input caused by actuator faults. Actuator faults are categorized into additive and multiplicative faults. According to their way of representation [29], [38], the fault input $\Delta u_f(t)=\left[\Delta wf_f\ \ \Delta vsv_f\right]^T\in\mathbb{R}^q$ is described by

$$\begin{cases}\Delta u_f^a(t)=\Phi_f^a(t)+\varrho_f^a(t),\\ \Delta u_f^m(t)=\Phi_f^m(t)\Delta u_c^m(t)+\varrho_f^m(t),\end{cases} \tag{2}$$

where the variables with superscripts a and m represent the case of actuators with additive faults and multiplicative faults. $\Delta u_c^m(t)$ and $\Delta u_c^a(t)$ that appears later are the commanded inputs of turbofan engines with multiplicative faults and additive faults, and the vector $\Phi_f^a(t)=\left[\phi_f^{a,1}(t)\ \phi_f^{a,2}(t)\right]^T\in\mathbb{R}^q$ and the matrix $\Phi_f^m(t)=diag(\phi_f^{m,1}(t),\phi_f^{m,2}(t))\in\mathbb{R}^{q\times q}$ represent the fault parameters, where the scalars $\phi_f^{a,j}(t)$ and $\phi_f^{m,j}(t)$ for $j\in 1,\ldots,q$ take values between -1 and 0, making it possible to represent partial actuator faults. The mixed error vectors $\varrho_f^a(t)=\left[\varrho_f^{a,1}(t)\ \varrho_f^{a,2}(t)\right]^T\in\mathbb{R}^q$ and $\varrho_f^m(t)=\left[\varrho_f^{m,1}(t)\ \varrho_f^{m,2}(t)\right]^T\in\mathbb{R}^q$ account for diagnosis errors, model inadequacy, and so on.

Remark 1: Note that the fault input in the fault-free case can also be represented as (2) with $\phi_f^{a,j}(t)=0$ and $\phi_f^{m,j}(t)=0$.

Remark 2: Experience has shown that faults are likely to occur alone [1]. Due to the presence of the first faulty actuator in the system, other faults may be triggered sequentially. We always have to consider which fault occurs first. Therefore, the single fault situation is considered in the design of the fault-tolerant system in practical applications.

B. POLYNOMIAL STATE-SPACE MODEL OF TURBOFAN ENGINES WITH ACTUATOR FAULTS

Consider the polynomial state-space model describing turbofan engines given by

$$\Delta\dot{x}(t)=\sum_{i=1}^{p}A_i\Delta x^{\{i\}}(t)+B_2\Delta u(t)+B_1d(t), \tag{3}$$

where $\Delta x(t)=\left[\Delta nl\ \ \Delta nh\right]^T\in\mathbb{R}^n$ denotes the low-pressure and high-pressure shaft speeds as the state vector, $\Delta x^{\{i\}}(t)=\left[\Delta nl^i\ \ \Delta nh^i\right]^T\in\mathbb{R}^n$ for $i=1,2,\ldots,p$, where p is the order of the state polynomial, $\Delta u(t)=\left[\Delta wf\ \ \Delta vsv\right]^T\in\mathbb{R}^q$ is

fuel flow and variable stator vanes as the actual input vector, $d(t) = \left[d_1(t)\ d_2(t)\right]^T \in \mathbb{R}^k$ is the various uncertain term due to model simplification, disturbances, and so on. The matrices have appropriate dimensions with $B_1 \in \mathbb{R}^{n\times k}$ and $A_i \in \mathbb{R}^{n\times n}$ for $i \in 1, 2, \ldots, p$. $B_2 \in \mathbb{R}^{n\times q}$ is full column rank and define its left inverse as B_{2L}^{-1}. In this paper, $n = k = q = 2$.

In the case of actuators with additive faults and multiplicative faults, according to (1) and (2), the actual inputs $\Delta u(t)$ can be represented by $\Delta u^a(t)$ and $\Delta u^m(t)$ in (4), respectively.

$$\begin{cases} \Delta u^a(t) = \Delta u_c^a(t) + \Phi_f^a(t) + \varrho_f^a(t), \\ \Delta u^m(t) = \left(I_q + \Phi_f^m(t)\right)\Delta u_c^m(t) + \varrho_f^m(t), \end{cases} \tag{4}$$

where the commanded inputs $\Delta u_c^a(t)$, $\Delta u_c^m(t)$, the fault parameters $\Phi_f^a(t)$, $\Phi_f^m(t)$, and the mixed error vectors $\varrho_f^a(t)$, $\varrho_f^m(t)$ are in (2).

C. THE OBJECTIVE OF THE CIFTC SYSTEM

This paper is expected to design an integrated CIFTC system for turbofan engines to improve the performance of turbofan engines with actuator faults. To indicate the performance, a fictitious performance vector $\kappa_f(t)$ is given and will be described later. Before proposing the specific objective, we define the following L_2 gain-like and nonlinear H_∞ fault-tolerant control performance specifications.

Definition 1 (L_2 Gain-Like): For turbofan engines with actuator faults (3) (4), $d(t)$, $\varrho_f(t)$ (represented by $\varrho_f^a(t)$ and $\varrho_f^m(t)$), $\kappa_f(t)$ are the uncertain term, the mixed error vector, and the fictitious performance vector, respectively. The closed-loop system is said to satisfy the L_2 gain-like performance, if there exist positive constants γ and δ such that

$$\int_0^T \kappa_f^T(t)\kappa_f(t)dt \le \int_0^T \left(\gamma^2 d^T(t)d(t) + \delta^2 \varrho_f^T(t)\varrho_f(t)\right)dt, \tag{5}$$

where γ and δ represent the limitations from the uncertain term and the mixed error vector to the fictitious performance, respectively.

Definition 2 (Nonlinear H_∞ Fault-Tolerant Control Performance Specifications): Nonlinear H_∞ fault-tolerant control performance specifications (NHFTCPS) require that the closed-loop system can make turbofan engines asymptotically track reference signals for $d(t) = 0$ and $\varrho_f(t) = 0$, and satisfy the L_2 gain-like performance with $\gamma > 0$ and $\delta > 0$ for $d(t) \neq 0$ and $\varrho_f(t) \neq 0$.

The objective of this paper is to design a CNN-based intelligent fault-tolerant control system for turbofan engines to ensure that NHFTCPS are achieved for given $\gamma > 0$ and $\delta > 0$.

Remark 3: The main difference between Definition 1 and L_2 gain is that a more general condition is defined here. The closed-loop fault-tolerant control system of turbofan engines has L_2 gain-like, which is represented as a multiple-input single-output map, from the inputs of $d(t)$ and $\varrho_f(t)$ to the defined penalty variable $\kappa_f(t)$. The closed-loop fault-tolerant control system satisfies the L_2 gain-like performance, which guarantees that the effects of $d(t)$ and $\varrho_f(t)$ on turbofan engines is finite and the upper bounds can be calculated.

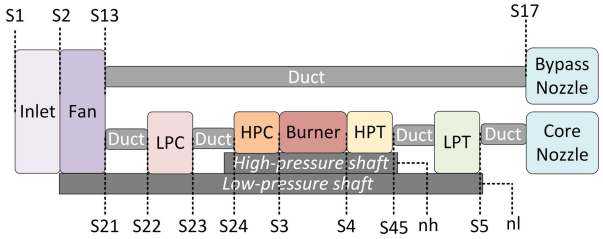

FIGURE 1. Schematic of the dual spool high bypass turbofan engine JT9D in T-MATS.

TABLE 2. Ten measurable gas-path variables of turbofan engines.

Symbol	Description
nl	low-pressure shaft speed
nh	high-pressure shaft speed
P_{17}	pressure before Bypass Nozzle
T_{17}	temperature before Bypass Nozzle
P_{21}	pressure after Fan
T_{21}	temperature after Fan
P_3	pressure before Burner
T_3	temperature before Burner
P_{45}	pressure after HPT
T_{45}	temperature after HPT

Remark 4: The notion of L_2-like gain in Definition 1 is to guarantee the robust performance of the closed-loop control system. Robustness is one of the basic functions of the designed control system for turbofan engines.

III. STRUCTURE OF CIFTC FOR TURBOFAN ENGINES

With the development of communication technologies, the operation data of turbofan engines can be acquired from the Quick Access Recorder (QAR) for safety analysis. This operation data includes specific gas-path data of turbofan engines, which can provide effective support for the safety and reliability analysis of the engine system [21], [39], [40]. The CIFTC system is developed according to the operation data from QAR of turbofan engines in the paper.

Figure 1 shows the schematic of the main components of the JT9D engine in T-MATS (the Toolbox for the Modeling and Analysis of Thermodynamic Systems), such as Fan, high-pressure compressor (HPC), Burner, high-pressure turbine (HPT), Bypass Nozzle, and so on. Furthermore, locations along the flow path are indicated by the station numbers, which can be used to analyze the overall operation of turbofan engines [37]. The gas-path data of turbofan engines contains useful operational information and has been used in component fault diagnosis [37], remaining useful life estimation [41], health monitoring [42], and so on. To provide the operation information of actuator faults, the difference between actual and normal sensor signals of the key engine stations is called gas-path total measurable fault information (GToMFI). The GToMFI is introduced into the design of the CIFTC system (see Table 2).

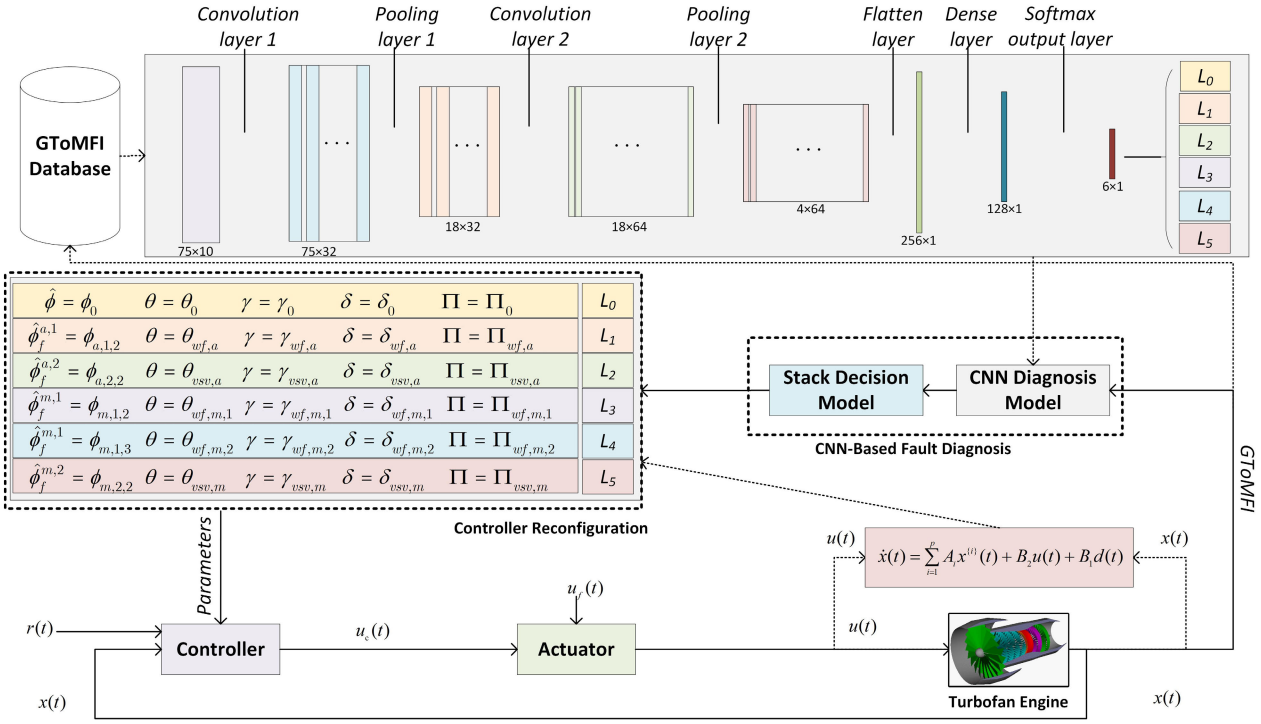

FIGURE 2. General scheme of the CIFTC for turbofan engines with actuator faults. ⇢ indicates the offline design process and → indicates the real-time online operation in the figure.

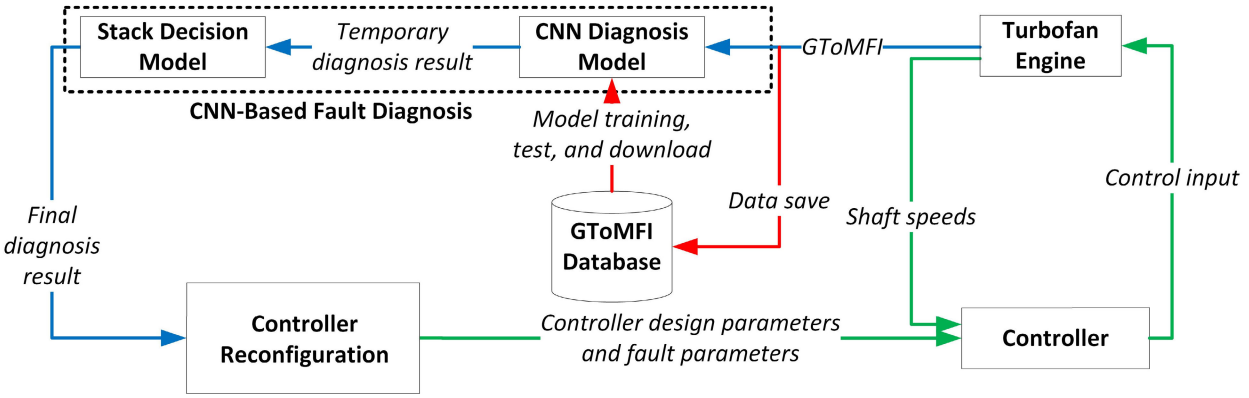

FIGURE 3. Working process of the CIFTC system for turbofan engine.

Figure 2 shows that the general scheme of the CIFTC system for turbofan engines. Similar to other fault-tolerant control systems, the proposed CIFTC system in the paper contains a turbofan engine, a CNN-based diagnosis module, a nonlinear fault-tolerant controller, and the corresponding reconfiguration unit. Based on the database of GToMFI, the CNN-based fault diagnosis module is to provide diagnosis results for the controller reconfiguration unit. According to the diagnosis results, the controller reconfiguration unit is to choose suitable controller parameters and reconfigure the existing nonlinear controller effectively. The reconfigured controller is to reduce the impacts of actuator faults on turbofan engines. These four parts need to work in harmony to complete fault-tolerant control tasks for turbofan engines under both normal and fault conditions.

The fault-tolerant control of the proposed system is implemented in three steps. The first step is the fault diagnosis process, in which the temporary diagnosis result is provided by the CNN diagnosis model and the final diagnosis result is provided by the stack decision model. In the second step, the fault parameters and controller design parameters are given by the controller reconfiguration unit according to the final diagnosis result. With these suitable parameters, the fault-tolerant controller provides the control input to the turbofan engine. In the third step, under the reconfigured fault-tolerant controller, the turbofan engine can provide new data to the GToMFI database for training, verifying, and saving the CNN diagnosis model. The completed working process of the CIFTC system for turbofan engine is illustrated in Fig. 3.

IV. CNN-BASED FAULT DIAGNOSIS

In this section, the CNN-based fault diagnosis module is developed in the CIFTC system for turbofan engines. In this module, the CNN diagnosis model and the stack decision model are designed in detail.

A. CNN DIAGNOSIS MODEL

As an effective deep learning method, CNN has been successfully utilized in various applications involving time series data, especially in control systems [37], [43]–[46]. Based on the GToMFI database, the CNN diagnosis model is designed including data processing, cross-entropy calculation, key neural layers such as convolutional layer, pooling layer, and fully connected layer, etc.

1) DATA PROCESSING

To normalize the GToMFI data, the min-max normalization method adopted from [47] is given by

$$\chi^* = \frac{\chi - \chi_{min}}{\chi_{max} - \chi_{min}} \tag{6}$$

where χ_{min} and χ_{max} denote the minimum and the maximum of the GToMFI data (represented by χ) of turbofan engines, and χ^* denotes the normalized value of χ.

Figure 4 shows that the GToMFI data is re-scaled within the range [0, 1] after normalization. The normalized GToMFI data is divided into several short segments with equal length by sliding-window sampling for feature extraction. To improve the correlation between adjacent segments, the sampling length of the segments is much large than the sliding step.

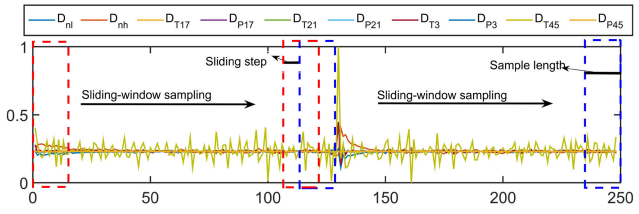

FIGURE 4. Segmentation of the GToMFI data by sliding-window sampling.

Through the above data processing, more and standard data samples are obtained for training and testing the CNN diagnosis model.

2) CONVOLUTIONAL LAYER

The convolutional layer contains a series of learnable kernels and parameters. The convolutional operation involves the application of dot products between the raw input data and the convolution kernels. The convolution process [47] with a nonlinear activation is described by

$$\zeta_h^{(b)} = ReLU\Big(\sum_{r=1}^{R} \alpha_h^{(b)} \otimes \chi_{(h-1)}^{(r)} + \beta_h^{(b)}\Big), \tag{7}$$

where $\zeta_h^{(b)}$ is the output of the b th kernel in the hth convolutional layer, $\chi_{(h-1)}^{(r)}$ is the r th output of the previous network layer, $\otimes$ represents the convolutional operator, $\alpha_h^{(b)}$ and $\beta_h^{(b)}$ denotes the weight and bias of the b th kernel of the h th convolutional layer, *ReLU* is the activation function Rectified Linear Unit.

3) POOLING LAYER

To avoid over-fitting, a pooling layer is often appended to a convolutional layer. The max-pooling operator is applied to each feature map separately by fusing nearby feature values into one value [48]. The max-pooling is given by

$$\xi_{h+1}^{(b)} = \max_{(v-1)w<y\le vw} \Big[\zeta_h^{(b)}(y)\Big], \tag{8}$$

where $\zeta_h^{(b)}(y)$ represents the y th value in the b th feature map of the h th layer, $\xi_{h+1}^{(b)}$ is the outcome in the b th feature map of the h+1 th pooling layer, w is the height of the pooling window.

4) FULLY-CONNECTED LAYER

After alternately stacking multiple convolutional layers and pooling layers, a flatten layer is followed to transform the extracted feature map into a one-dimensional array [49]. The softmax activation function is used in the output layer for normalizing the result of the fully-connected layer to meet probability distribution [50]. The output of the softmax function is defined by

$$P_l = \begin{bmatrix} P(L_l = 1) \\ \cdots \\ P(L_l = g) \\ \cdots \\ P(L_l = z) \end{bmatrix}^T = \frac{1}{\sum_{g=1}^{z} e^{\upsilon_g}} \begin{bmatrix} e^{\upsilon_1} \\ \cdots \\ e^{\upsilon_g} \\ \cdots \\ e^{\upsilon_z} \end{bmatrix}^T, \tag{9}$$

where υ_g is the input of the softmax function for $g = 1, 2, \cdots, z$, $P_l = \begin{bmatrix} P_l^{(1)} & \cdots & P_l^{(g)} & \cdots & P_l^{(z)} \end{bmatrix}$ is the output value of the l th sample after normalization by the softmax function, $P(L_l = g)$ is the probability value of the l th sample belonging to label g. The label corresponding to the maximum value of each row in P_l is the CNN diagnosis result.

5) CROSS-ENTROPY LOSS CALCULATION

By comparing the normalized diagnosis result with the actual label of the corresponding sample, the loss error of the CNN diagnosis model can be calculated. To represent the loss error, the cross-entropy loss function [51] is defined as follows

$$J = -\frac{1}{s}\Big(\sum_{l=1}^{s}\sum_{g=1}^{z} \mathcal{F}\{\bar{L}_l = g\} log\big(P(L_l = g)\big)\Big), \tag{10}$$

where l represents the l th training sample (the total number of training sample is s), g represents the g th label (the total number of labels is z), and $\mathcal{F}\{\bar{L}_l = g\}$ is a logical indication function, returning 1 if the statement is true, and 0 if the statement is false.

In this paper, the Adam optimization algorithm is used for minimizing the cross-entropy loss function J according to the rule of error back-propagation, where the learning rate

can automatically adjust its step length according to the local error surface of the mini-batch sample [52]. The learnable parameters of the CNN diagnosis model are updated in the training process.

Figure 5 shows the flow chart of the CNN diagnosis model used for monitoring the operation of actuators. In addition to the important layers mentioned above, a BatchNormalization layer is added after the convolutional layer to make the data in the current training batch follow a normal distribution. The BatchNormalization was introduced back in 2014 in the second version of GoogLeNet by Szegedy *et al.* [53]. The introduction of the BatchNormalization layer not only accelerates the convergence speed in training but also allows for higher learning rates. Hence. the CNN diagnosis model can prevent overfitting and improve generalization capability. The designed CNN diagnosis model can provide real-time monitoring for the engine operation.

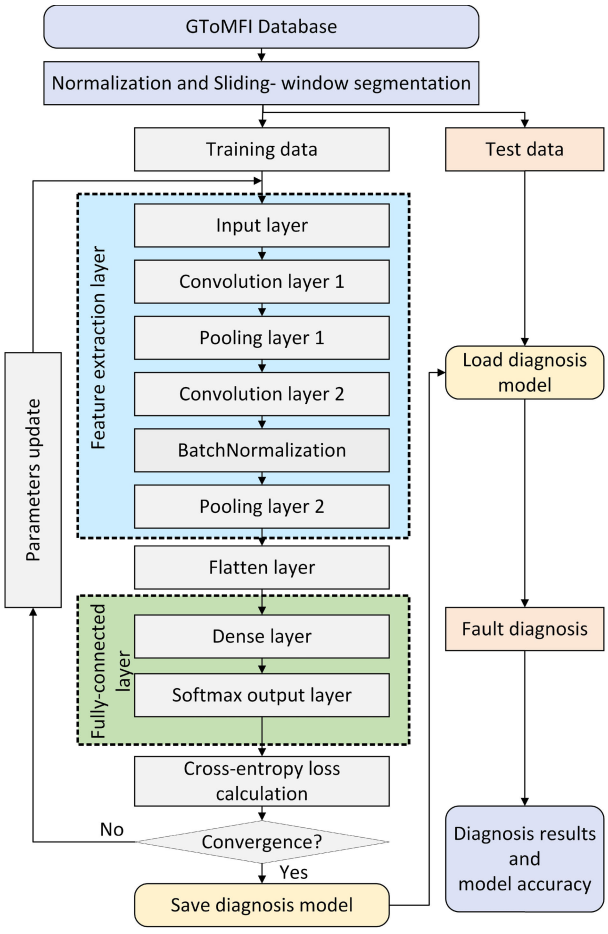

FIGURE 5. The flow chart of the CNN diagnosis model.

B. STACK DECISION MODEL

According to the monitoring results provided by the CNN diagnosis model, a stack decision model is developed to give the final fault determination. The specific expression of the stack decision model is given by

$$\grave{L}_K = \begin{cases} L_K, & \text{if } L_{sf,K} = L_K * E_{sf} \\ \grave{L}_{K-1}, & \text{others,} \end{cases} \tag{11}$$

where L_K is the monitoring result provided by the CNN diagnosis model at the Kth sampling time, $L_{sf,K} = \left[L_{K-sf+1}\ L_{K-sf+2}\ \ldots\ L_K\right]^T \in \mathbb{R}^{sf}$ is the stack decision vector composed of the monitoring results of the sampling time from $K-sf+1$ to K, $sf > 1$ represents the stack length of the stack decision model, E_{sf} is a sf-dimensional column vector with all elements of 1, $\grave{L}_K$ and $\grave{L}_{K-1}$ are the final fault determinations at the K th sampling time and previous moment, respectively.

The stack diagnosis model and the CNN diagnosis model constitute the CNN-based diagnosis module of the CIFTC system. The module can provide the final fault determinations for the nonlinear fault-tolerant controller in the CIFTC system for turbofan engines.

Remark 5: The expression of the stack decision model in (11) means that the previous fault determination is changed only if sf consecutive temporary diagnosis results are consistent. The selection of the stack length needs to consider the acceptable fault-tolerance time of the control system for turbofan engines.

Remark 6: The CNN-based diagnosis model is to extract the information of actuator faults from the gas-path data, which helps relax the accuracy requirements of the mathematical description of turbofan engines for the whole fault-tolerant control system. Meanwhile, in addition to the controlled shaft speeds, other gas-path data is also used to provide the fault information of turbofan engines, which can improve the reliability and security of the CIFTC system.

V. NONLINEAR FAULT-TOLERANT CONTROL

In this section, the nonlinear fault-tolerant controller of the CIFTC system is designed to achieve NHFTCPS. To tackle the nonlinearity of turbofan engines, a solvable Hamilton-Jacobi-Issacs (HJI) inequality is constructed by a Lyapunov function to obtain the nonlinear robust fault-tolerant controller. Firstly, the tracking error dynamic model of the closed-loop fault-tolerant control system is established. Based on the tracking error dynamics, the nonlinear fault-tolerant control problem of turbofan engines is converted into the stability and robustness analysis with establishing corresponding criteria. Then, we propose a suboptimal nonlinear H_∞ control problem in Theorem 1, and then construct an analytical solution and a sufficient condition to the suboptimal nonlinear H_∞ control problem in Theorem 2. Finally, the solution of the nonlinear fault-tolerant controller is given in terms of linear matrix inequalities.

A. NONLINEAR ROBUST FAULT-TOLERANT CONTROL DESIGN

According to the final fault determination provided by the CNN-based fault diagnosis module, the fault parameters can be obtained. In the case of the additive and multiplicative

faults, the matrix and vector of the fault parameters can be expressed as

$$\widehat{\Phi}_f^a(t) = \left[\widehat{\phi}_f^{a,1}(t)\ \widehat{\phi}_f^{a,2}(t)\right]^T \in \mathbb{R}^q, \tag{12}$$

$$\widehat{\Phi}_f^m(t) = diag(\widehat{\phi}_f^{m,1}(t), \widehat{\phi}_f^{m,2}(t)) \in \mathbb{R}^{q\times q}. \tag{13}$$

The corresponding mixed error vectors are presented by $\widehat{\varrho}_f^a(t)$ and $\widehat{\varrho}_f^m(t)$, respectively.

Based on (4), a uniform model of the actual inputs of turbofan engines is formulated by

$$\Delta u(t) = \widehat{\Theta}_f(t)\Delta\widehat{\omega}_f(t)+\varrho_f(t), \tag{14}$$

where $\widehat{\Theta}_f(t) = \widehat{\Theta}_f^a(t) = I_q$, $\Delta\widehat{\omega}_f(t) = \Delta\widehat{\omega}_f^a(t) = \Delta u_c^a(t)+\widehat{\Phi}_f^a(t)$, and $\varrho_f(t) = \widehat{\varrho}_f^a(t) = \varrho_f^a(t)+\left(\Phi_f^a(t)-\widehat{\Phi}_f^a(t)\right)$ in the additive fault case, $\widehat{\Theta}_f(t) = \widehat{\Theta}_f^m(t) = I_q+\widehat{\Phi}_f^m(t)$, $\Delta\widehat{\omega}_f(t) = \Delta\widehat{\omega}_f^m(t) = \Delta u_c^m(t)$, and $\varrho_f(t) = \widehat{\varrho}_f^m(t) = \varrho_f^m(t)+\left(\Phi_f^m(t)-\widehat{\Phi}_f^m(t)\right)\Delta u_c^m(t)$ in the multiplicative fault case.

Substitute $\Delta u(t)$ in (14) into the polynomial state-space model of turbofan engines in (3) yields

$$\Delta\dot{x}(t) = \sum_{i=1}^{p} A_i\Delta x^{\{i\}}(t)+B_2\left(\widehat{\Theta}_f(t)\Delta\widehat{\omega}_f(t)+\varrho_f(t)\right) +B_1 d(t) \tag{15}$$

where $\Delta x(t)$ and $d(t)$ are the state vector and the various uncertain term, A_i, B_2, and B_1 are the system matrices in (3).

Given that $\Delta r(t) \in \mathbb{R}^n$ is the bounded reference signal, the tracking error $\Delta e(t)$ of turbofan engines is defined as

$$\Delta e(t) \triangleq \Delta x(t)-\Delta r(t), \tag{16}$$

To eliminate the steady-state error, the integral action of the tracking error $\Delta\sigma(t)$ of turbofan engines is introduced into the closed-loop control system by

$$\Delta\sigma(t) \triangleq \int_0^t \Delta e(\tau)d\tau. \tag{17}$$

The derivatives of the tracking error and its integral with respect to t are given by

$$\Delta\dot{\sigma}(t) = \Delta e(t), \tag{18}$$

$$\Delta\dot{e}(t) = \sum_{i=1}^{p} A_i\Delta e^{\{i\}}(t)+B_2\Delta\widehat{u}_e^f(t)+B_1 d(t), \tag{19}$$

where $\Delta\widehat{u}_e^f(t)$ in (20) is the inputs of the error dynamics of turbofan engines.

$$\Delta\widehat{u}_e^f(t) = -B_2{}^{-1}\Big(\sum_{i=1}^{p} A_i\Delta x^{\{i\}}(t)-\sum_{i=1}^{p} A_i\Delta e^{\{i\}}(t)-\Delta\dot{r}(t)\Big) +\widehat{\Theta}_f(t)\Delta\widehat{\omega}_f(t)+\varrho_f(t) \tag{20}$$

Refer to (18) and (19) together as the error dynamical model of the closed-loop system for turbofan engines,

$$\Delta\dot{\zeta}_1(t) = \Upsilon\Delta\zeta(t)+\Xi\Delta\widehat{u}_e^f(t)+\Omega d(t), \tag{21}$$

where $\Delta\zeta_1(t) = \left[\Delta\sigma(t)^T\ \Delta e(t)^T\right]^T \in \mathbb{R}^{2n}$ is the state vector, $\Delta\zeta(t) = \left[\Delta\zeta_1(t)^T\ \ldots\ \Delta\zeta_i(t)^T\ \ldots\ \Delta\zeta_p(t)^T\right]^T \in \mathbb{R}^{2np}$ is the polynomial state vector, where $\Delta\zeta_i(t) = \left[\Delta\sigma^{\{i\}}(t)^T\ \Delta e^{\{i\}}(t)^T\right]^T \in \mathbb{R}^{2n}$ for $i = 1, 2, \ldots, p$, $d(t) = \left[d_1(t)\ d_2(t)\right]^T \in \mathbb{R}^k$ is the uncertain term due to model simplification, disturbance, and so on. $\Delta\widehat{u}_e^f(t)$ is the input vector rewritten as

$$\Delta\widehat{u}_e^f(t) = \widehat{\Theta}_f(t)\Delta\widehat{\omega}_e^f(t)+\varrho_f(t), \tag{22}$$

where $\widehat{\Theta}_f(t)$ and $\varrho_f(t)$ are in (14), and

$$\Delta\widehat{\omega}_e^f(t) = \widehat{\Theta}_f^{-1}(t)B_2{}^{-1}\Big(\sum_{i=1}^{p} A_i\Delta x^{\{i\}}(t)-\sum_{i=1}^{p} A_i\Delta e^{\{i\}}(t)-\Delta\dot{r}(t)\Big) +\Delta\widehat{\omega}_f(t).$$

The system matrices of (21) are given by

$$\Omega = \begin{bmatrix}0_{n\times k}\\ B_1\end{bmatrix} \in \mathbb{R}^{2n\times k}, \quad \Xi = \begin{bmatrix}0_{n\times q}\\ B_2\end{bmatrix} \in \mathbb{R}^{2n\times q},$$
$$\Upsilon = \begin{bmatrix}\Upsilon_1\ \ldots\ \Upsilon_i\ \ldots\ \Upsilon_p\end{bmatrix} \in \mathbb{R}^{2n\times 2np},$$

where

$$\Upsilon_1 = \begin{bmatrix}0_n & I_n\\ 0_n & A_1\end{bmatrix} \in \mathbb{R}^{2n\times 2n}, \quad \Upsilon_i = \begin{bmatrix}0_n & 0_n\\ 0_n & A_i\end{bmatrix} \in \mathbb{R}^{2n\times 2n},$$
$$i = 2, 3, \ldots, p.$$

To indicate the control performance of the closed-loop system for turbofan engines, the fictitious performance vector $\kappa_f(t)$ in (5) is defined by

$$\kappa_f(t) \triangleq \begin{bmatrix}\mathcal{H}\left(\Delta\zeta_1\right)\\ \theta\Delta\widehat{\omega}_e^f(t)\end{bmatrix} \tag{23}$$

where θ is a positive coefficient and $\mathcal{H}\left(\Delta\zeta_1\right)$ is a cost function of the state of the error dynamical model.

Assumption 1: The cost function $\mathcal{H}\left(\Delta\zeta_1\right)$ in (23) satisfies

$$\mathcal{H}^T\left(\Delta\zeta_1\right)\mathcal{H}\left(\Delta\zeta_1\right) \le \Delta\zeta^T(t)\Pi\Delta\zeta(t), \tag{24}$$

where $\Pi \in \mathbb{R}^{2np\times 2np}$ is a symmetric positive definite matrix.

Remark 7: In Assumption 1, $\mathcal{H}^T\left(\Delta\zeta_1\right)\mathcal{H}\left(\Delta\zeta_1\right)$ is less than or equal to a polynomial of a certain degree. This is a necessary condition for Theorem 1 in this paper.

Remark 8: As shown in (14), the commanded inputs $\Delta u_c^a(t)$ and $\Delta u_c^m(t)$ are included in $\Delta\widehat{\omega}_f(t)$. According to (22), $\Delta\widehat{\omega}_f(t)$ is a part of $\Delta\widehat{\omega}_e^f(t)$. These mean that once $\Delta\widehat{\omega}_e^f(t)$ is given, the fault-tolerant controllers of the CIFTC system for turbofan engines can be designed.

To satisfy the NHFTCPS of the closed-loop system of turbofan engines, firstly, we propose

$$\Delta\widehat{\omega}_e^f(t) = -\widehat{\Theta}_f(t)\Xi^T\Gamma(1, p)\Lambda\Psi\Delta\zeta(t). \tag{25}$$

Then, in case of actuators with additive faults and multiplicative faults, we design nonlinear robust fault-tolerant controllers $\Delta u_c^a(t)$ and $\Delta u_c^m(t)$ in (26) and (27) for the CIFTC system, respectively,

$$\Delta u_c^a(t) = \eta(t)-\Xi^T\Gamma(1, p)\Lambda\Psi\Delta\zeta(t)-\widehat{\Phi}_a(t), \tag{26}$$

$$\Delta u_c^m(t) = -\left(I_m+\widehat{\Phi}_m(t)\right)\Xi^T\Gamma(1,p)\Lambda\Psi\Delta\zeta(t) +\left(I_m+\widehat{\Phi}_m(t)\right)^{-1}\eta(t), \quad (27)$$

where

$$\eta(t) = -B_{2_L}^{-1}\Big(\sum_{i=1}^{p}A_i\Delta x^{\{i\}}(t)-\sum_{i=1}^{p}A_i\Delta e^{\{i\}}(t)-\Delta\dot{r}(t)\Big), \quad (28)$$

the $\Lambda = \begin{bmatrix} \Lambda_1 & 0_{2n\times 2n(p-1)} \\ 0_{2n(p-1)\times 2n} & \Lambda_2 \end{bmatrix} \in \mathbb{R}^{2np\times 2np}$ is a symmetric positive definite matrix, Λ_1, Λ_2 are $2n\times 2n$ and $2n(p-1)\times 2n(p-1)$ symmetric positive definite matrices. $\Psi \in \mathbb{R}^{2np\times 2np}$ is a square matrix. The conditions that the matrices Λ and Ψ need to satisfy will be given in Theorem 2 later. $\Gamma(1,p) = \left[I_{2n}\ 0_{2n\times 2n(p-1)}\right] \in \mathbb{R}^{2n\times 2np}$. $\widehat{\Phi}_a(t)$ and $\widehat{\Phi}_m(t)$ are the matrix and vector of fault parameters provided by the CNN-based fault diagnosis module.

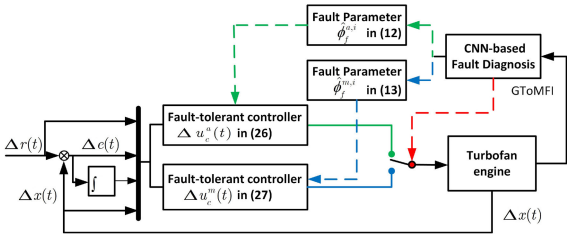

FIGURE 6. Block diagram of the fault-tolerant controllers of the CIFTC system for turbofan engines.

Finally, the block diagram of the fault-tolerant controllers of the CIFTC system are shown in Fig. 6. The nonlinear fault-tolerant controllers are reconfigured flexibly according to the fault parameters provided by the CNN-based fault diagnosis module.

Remark 9: The proposed nonlinear fault-tolerant controller is a typical active fault-tolerant controller. Based on the CNN-based diagnosis module, the proposed fault-tolerant controller is designed as a part of an integrated fault-tolerant control system. The actuator faults of the value within a certain range belong to the same fault mode. The design method of the proposed controller can relax the accuracy requirement of the diagnosis module and avoid reconfiguring the controller of turbofan engines frequently in the case of minor changes of the fault value.

B. STABILITY AND CONTROL PERFORMANCE

Theorem 1: For the error dynamics of the closed-loop system for turbofan engines with actuator faults in (21), $d(t)$, $\varrho_f(t)$ in (22), $\kappa_f(t)$ in (23) are the uncertain term, the mixed error vector, and the fictitious performance vector, respectively. For given positive coefficients θ, γ, and δ, if there is a continuously differentiable positive definite function $V(t)$ with $V(0) = 0$ for $\Delta\zeta_1(0) = 0$ such that (29) holds,

$$\frac{1}{4\delta^2}\frac{\partial^T V(t)}{\partial\Delta\zeta_1(t)}\Xi\Xi^T\frac{\partial V(t)}{\partial\Delta\zeta_1(t)}+\mathcal{H}^T\left(\Delta\zeta_1\right)\mathcal{H}\left(\Delta\zeta_1\right) +\frac{\partial^T V(t)}{\partial\Delta\zeta_1(t)}\Upsilon\Delta\zeta(t)+\frac{\partial^T V(t)}{\partial\Delta\zeta_1(t)}\Xi\widehat{\Theta}_f(t)\Delta\widehat{\omega}_e^f(t) +\frac{1}{4\gamma^2}\frac{\partial^T V(t)}{\partial\Delta\zeta_1(t)}\Omega\Omega^T\frac{\partial V(t)}{\partial\Delta\zeta_1(t)}+\kappa_f^T(t)\kappa_f(t) +\theta^2\Delta\widehat{\omega}_e^{f\,T}(t)\Delta\widehat{\omega}_e^f(t)\le 0 \quad (29)$$

then the NHFTCPS in Definition 2 can be satisfied by the proposed CIFTC system for turbofan engines.

Proof: A scalar function $\mathcal{G}(t)$ is given by

$$\mathcal{G}(t) \triangleq \frac{dV(t)}{dt}+\kappa_f^T(t)\kappa_f(t)-\gamma^2 d^T(t)d(t)-\delta^2\varrho_f^T(t)\varrho_f(t). \quad (30)$$

Considering $V(t)$ is a function of $\Delta\zeta_1(t)$, (30) can be written as

$$\begin{aligned}\mathcal{G}(t) &= \frac{\partial^T V(t)}{\partial\Delta\zeta_1(t)}\Big(\Upsilon\Delta\zeta(t)+\Omega d(t)+\Xi\big(\widehat{\Theta}_f(t)\Delta\widehat{\omega}_e^f(t)+\varrho_f(t)\big)\Big) +\kappa_f^T(t)\kappa_f(t)-\gamma^2 d^T(t)d(t)-\delta^2\varrho_f^T(t)\varrho_f(t)\\ &= \frac{\partial^T V(t)}{\partial\Delta\zeta_1(t)}\Xi\widehat{\Theta}_f(t)\,\Delta\widehat{\omega}_e^f(t)+\frac{\partial^T V(t)}{\partial\Delta\zeta_1(t)}\Upsilon\Delta\zeta(t) +\frac{\partial^T V(t)}{\partial\Delta\zeta_1(t)}\Omega d(t)+\mathcal{H}^T\left(\Delta\zeta_1\right)\mathcal{H}\left(\Delta\zeta_1\right)\\ &\quad+\frac{\partial^T V(t)}{\partial\Delta\zeta_1(t)}\Xi\varrho_f(t)+\theta^2\Delta\widehat{\omega}_e^{f\,T}(t)\Delta\widehat{\omega}_e^f(t) -\gamma^2 d^T(t)d(t)-\delta^2\varrho_f^T(t)\varrho_f(t),\end{aligned} \quad (31)$$

which is a quadratic function of $d(t)$ and $\varrho_f(t)$. Therefore, equation (31) has the maximum value at $d^*(t)$ and $\varrho_f^*(t)$ (for a fixed $V(t)$).

$$d^*(t) = \frac{1}{2\gamma^2}\Omega^T\frac{\partial V(t)}{\partial\Delta\zeta_1(t)}, \quad (32)$$

$$\varrho_f^*(t) = \frac{1}{2\delta^2}\Xi^T\frac{\partial V(t)}{\partial\Delta\zeta_1(t)}. \quad (33)$$

Taking $d^*(t)$ and $\varrho_f^*(t)$ into (31) yields

$$\begin{aligned}\mathcal{G}(t) &\le \frac{1}{4\delta^2}\frac{\partial^T V(t)}{\partial\Delta\zeta_1(t)}\Xi\Xi^T\frac{\partial V(t)}{\partial\Delta\zeta_1(t)}+\mathcal{H}^T\left(\Delta\zeta_1\right)\mathcal{H}\left(\Delta\zeta_1\right)\\ &\quad+\frac{\partial^T V(t)}{\partial\Delta\zeta_1(t)}\Upsilon\Delta\zeta(t)+\frac{\partial^T V(t)}{\partial\Delta\zeta_1(t)}\Xi\widehat{\Theta}_f(t)\Delta\widehat{\omega}_e^f(t)\\ &\quad+\frac{1}{4\gamma^2}\frac{\partial^T V(t)}{\partial\Delta\zeta_1(t)}\Omega\Omega^T\frac{\partial V(t)}{\partial\Delta\zeta_1(t)}+\kappa_f^T(t)\kappa_f(t)\\ &\quad+\theta^2\Delta\widehat{\omega}_e^{f\,T}(t)\Delta\widehat{\omega}_e^f(t)\\ &\le 0.\end{aligned} \quad (34)$$

Integrating (34) yields

$$\int_0^T\kappa_f^T(t)\kappa_f(t)dt-\gamma^2\int_0^T d^T(t)d(t)dt +V(T)-V(0)-\delta^2\int_0^T\varrho_f^T(t)\varrho_f(t)dt\le 0. \quad (35)$$

According to $V(T) > 0$ and $V(0) = 0$ for $\Delta\zeta_1(0) = 0$, rearranging terms yields

$$\begin{aligned}\int_0^T \kappa_f^T(t)\kappa_f(t)dt &\le \int_0^T \left(\gamma^2 d^T(t)d(t)+\delta^2\varrho_f^T(t)\varrho_f(t)\right)dt - V(T)\\ &\le \int_0^T \left(\gamma^2 d^T(t)d(t)+\delta^2\varrho_f^T(t)\varrho_f(t)\right)dt. \end{aligned} \tag{36}$$

Thus, the closed-loop control system of turbofan engines satisfies the L_2 gain-like performance with $\gamma > 0$ and $\delta > 0$ for nonzero $d(t)$ and $\sigma_f(t)$ with $\gamma > 0$ and $\delta > 0$.

Moreover, if $d(t) = 0$ and $\varrho_f(t) = 0$, equation (34) can be rewritten as

$$\begin{aligned}&\dot V(t)+\kappa_f^T(t)\kappa_f(t)-\gamma^2 d^T(t)d(t)-\delta^2\varrho_f^T(t)\varrho_f(t)\\ &\quad= \dot V(t)+\mathcal{H}^T\left(\Delta\zeta_1\right)\mathcal{H}\left(\Delta\zeta_1\right)+\theta^2\Delta\widehat{\omega}_e^{fT}(t)\Delta\widehat{\omega}_e^f(t)\\ &\quad\le 0\end{aligned} \tag{37}$$

Because of Assumption 1, $\dot V(t) < 0$ expect at $\Delta\zeta_1(0) = 0$. Hence, the error dynamics of the closed-loop system of turbofan engines with actuator faults is locally asymptotically stable for $d(t) = 0$ and $\varrho_f(t) = 0$, which means that the controlled outputs of turbofan engines by the CIFTC system can asymptotically track reference signals for $d(t) = 0$ and $\varrho_f(t) = 0$.

The proof is completed.

Theorem 2: For given positive constants θ, γ, and δ, if there exists a symmetric positive definite matrix $\Lambda = \begin{bmatrix}\Lambda_1 & 0_{2n\times 2n(p-1)}\\ 0_{2n(p-1)\times 2n} & \Lambda_2\end{bmatrix} \in \mathbb{R}^{2np\times 2np}$ and a square matrix $\Psi \in \mathbb{R}^{2np\times 2np}$ that satisfy

$$\begin{aligned}&\Lambda\Gamma^T(1,p)\Upsilon-\Lambda\Gamma^T(1,p)\Xi\widehat{\Theta}_f^2(t)\Xi^T\Gamma(1,p)\Lambda\Psi\\ &\quad+\Upsilon^T\Gamma(1,p)\Lambda-\Psi^T\Lambda\Gamma^T(1,p)\Xi\widehat{\Theta}_f^2(t)\Xi^T\Gamma(1,p)\Lambda\\ &\quad+2\theta^2\Psi^T\Lambda\Gamma^T(1,p)\Xi\widehat{\Theta}_f^2(t)\Xi^T\Gamma(1,p)\Lambda\Psi+2\Pi\\ &\quad+\frac{1}{2\gamma^2}\Lambda\Gamma^T(1,p)\Omega\Omega^T\Gamma(1,p)\Lambda\\ &\quad+\frac{1}{2\delta^2}\Lambda\Gamma^T(1,p)\Xi\Xi^T\Gamma(1,p)\Lambda \le 0,\end{aligned} \tag{38}$$

then the NHFTCPS in Definition 2 can be satisfied by the proposed CIFTC system for turbofan engines.

Proof: Consider the Lyapunov function candidate

$$V(t) = \frac{1}{2}\Delta\zeta_1^T(t)\Lambda_1\Delta\zeta_1(t), \tag{39}$$

where $\Lambda_1 \in \mathbb{R}^{2n\times 2n}$ is a symmetric positive definite matrix. The partial derivative of $V(t)$ with respect to $\Delta\zeta_1(t)$ is given by

$$\frac{\partial V(t)}{\partial\Delta\zeta_1(t)} = \Gamma(1,p)\Lambda\Delta\zeta(t), \tag{40}$$

where $\Lambda = \begin{bmatrix}\Lambda_1 & 0_{2n\times 2n(p-1)}\\ 0_{2n(p-1)\times 2n} & \Lambda_2\end{bmatrix}$ is a symmetric positive definite matrix.

Taking $\partial V(t)/\partial\Delta\zeta_1(t)$ in (40), $\Delta\widehat{\omega}_e^f(t)$ in (25), and Assumption 1 in (24) into (29) yields

$$\begin{aligned}&\frac{1}{4\delta^2}\frac{\partial^T V(t)}{\partial\Delta\zeta_1(t)}\Xi\Xi^T\frac{\partial V(t)}{\partial\Delta\zeta_1(t)}+\mathcal{H}^T\left(\Delta\zeta_1\right)\mathcal{H}\left(\Delta\zeta_1\right)\\ &\quad+\frac{\partial^T V(t)}{\partial\Delta\zeta_1(t)}\Upsilon\Delta\zeta(t)+\frac{\partial^T V(t)}{\partial\Delta\zeta_1(t)}\Xi\widehat{\Theta}_f(t)\Delta\widehat{\omega}_e^f(t)\\ &\quad+\frac{1}{4\gamma^2}\frac{\partial^T V(t)}{\partial\Delta\zeta_1(t)}\Omega\Omega^T\frac{\partial V(t)}{\partial\Delta\zeta_1(t)}+\kappa_f^T(t)\kappa_f(t)\\ &\quad+\theta^2\Delta\widehat{\omega}_e^{fT}(t)\Delta\widehat{\omega}_e^f(t)\\ &\le \theta^2\Delta\zeta^T(t)\Psi^T\Lambda\Gamma^T(1,p)\Xi\widehat{\Theta}_f^2(t)\Xi^T\Gamma(1,p)\Lambda\Psi\Delta\zeta(t)\\ &\quad+\Delta\zeta^T(t)\Lambda\Gamma^T(1,p)\Upsilon\Delta\zeta(t)+\Delta\zeta^T(t)\Pi\Delta\zeta(t)\\ &\quad-\Delta\zeta^T(t)\Lambda\Gamma^T(1,p)\Xi\widehat{\Theta}_f^2(t)\Xi^T\Gamma(1,p)\Lambda\Psi\Delta\zeta(t)\\ &\quad+\frac{1}{4\gamma^2}\Delta\zeta^T(t)\Lambda\Gamma^T(1,p)\Omega\Omega^T\Gamma(1,p)\Lambda\Delta\zeta(t)\\ &\quad+\frac{1}{4\delta^2}\Delta\zeta^T(t)\Lambda\Gamma^T(1,p)\Xi\Xi^T\Gamma(1,p)\Lambda\Delta\zeta(t)\\ &= \frac{1}{2}\Delta\zeta^T(t)\Big(\Lambda\Gamma^T(1,p)\Upsilon\\ &\quad-\Lambda\Gamma^T(1,p)\Xi\widehat{\Theta}_f^2(t)\Xi^T\Gamma(1,p)\Lambda\Psi\\ &\quad+\Upsilon^T\Gamma(1,p)\Lambda-\Psi^T\Lambda\Gamma^T(1,p)\Xi\widehat{\Theta}_f^2(t)\Xi^T\Gamma(1,p)\Lambda\\ &\quad+2\theta^2\Psi^T\Lambda\Gamma^T(1,p)\Xi\widehat{\Theta}_f^2(t)\Xi^T\Gamma(1,p)\Lambda\Psi+2\Pi\\ &\quad+\frac{1}{2\gamma^2}\Lambda\Gamma^T(1,p)\Omega\Omega^T\Gamma(1,p)\Lambda\\ &\quad+\frac{1}{2\delta^2}\Lambda\Gamma^T(1,p)\Xi\Xi^T\Gamma(1,p)\Lambda\Big)\Delta\zeta(t)\\ &\le 0.\end{aligned} \tag{41}$$

Therefore, Ψ and Λ satisfying (38) can guarantee that the $V(t)$ in (39) is a solution to (29). Hence, the NHFTCPS in Definition 2 can be satisfied by the proposed CIFTC system for turbofan engines.

The proof is completed.

Remark 10: To obtain the key matrices Λ and Ψ of the nonlinear robust fault-tolerant controllers in (27) and (28), we define a symmetric positive definite symmetric matrix $\breve\Lambda = \Lambda^{-1}$ and a square matrix $\breve\Psi = \Lambda\Psi\Lambda^{-1}$. The inequality (38) is multiplied by $\breve\Lambda$ both the sides, which can be written as

$$\begin{aligned}&\breve\Lambda\times(38)\times\breve\Lambda\\ &\quad= \Gamma^T(1,p)\Upsilon\breve\Lambda-\Gamma^T(1,p)\Xi\widehat{\Theta}_f^2(t)\Xi^T\Gamma(1,p)\breve\Psi\\ &\quad+\breve\Lambda\Upsilon^T\Gamma(1,p)-\breve\Psi^T\Gamma^T(1,p)\Xi\widehat{\Theta}_f^2(t)\Xi^T\Gamma(1,p)\\ &\quad+2\theta^2\breve\Psi^T\Gamma^T(1,p)\Xi\widehat{\Theta}_f^2(t)\Xi^T\Gamma(1,p)\breve\Psi\\ &\quad+\frac{1}{2\gamma^2}\Gamma^T(1,p)\Omega\Omega^T\Gamma(1,p)+2\breve\Lambda\Pi\breve\Lambda\\ &\quad+\frac{1}{2\delta^2}\Gamma^T(1,p)\Xi\Xi^T\Gamma(1,p)\\ &\quad\le 0.\end{aligned} \tag{42}$$

According to Schur complement lemma, (42) can take the form of (43), as shown at the bottom of the next page.

TABLE 3. The detail hyper-parameters of the CNN diagnosis model.

Layer type	Parameters setting	Output Shape	Parameter amount
Input layer	[batch, 75, 10]	[batch, 75, 10]	0
Convolution layer 1	Filter = [6, 32], padding = 'same', strides = 1, activation = 'ReLU'	[batch, 75, 32]	1952
Max-Pooling layer 1	Pooling size = 4, padding = 'valid', strides = 1	[batch, 18, 32]	0
Convolution layer 2	Filter = [4, 64], padding = 'same', strides = 1, activation = 'ReLU'	[batch, 18, 64]	8256
BatchNormalization	Axis = -1, epsilon = 10^{-6}, momentum = 0.9, training = 'True'	[batch, 18, 64]	256
Max-Pooling layer 2	Pooling size = 4, padding = 'valid', strides = 1	[batch, 4, 64]	0
Flatten layer	to 1-D shape	[batch, 256]	0
Dense layer	128 hidden layer neuron nodes, activation = 'ReLU'	[batch, 128]	32896
Softmax output layer	Softmax activation function	[batch, 6]	774

where

$$\begin{aligned} O_1(\breve{\Lambda},\breve{\Psi}) &= \Gamma^T(1,p)\Upsilon\breve{\Lambda}+\breve{\Lambda}\Upsilon^T\Gamma(1,p) \\ &\quad -\breve{\Psi}^T\Gamma^T(1,p)\Xi\widehat{\Theta}_f^2(t)\Xi^T\Gamma(1,p) \\ &\quad -\Gamma^T(1,p)\Xi\widehat{\Theta}_f^2(t)\Xi^T\Gamma(1,p)\breve{\Psi}, \\ O_2 &= \sqrt{\Gamma^T(1,p)\Omega\Omega^T\Gamma(1,p)}, \\ O_3 &= \sqrt{\Gamma^T(1,p)\Xi\Xi^T\Gamma(1,p)}, \\ O_4 &= \sqrt{2\Pi}, \end{aligned}$$

and (*) denotes the symmetric term.

VI. SIMULATION RESULTS

In this section, the effectiveness of the proposed CIFTC system is verified for turbofan engines. The diagnosed and controlled object is the component level model of the dynamic dual spool high bypass engine JT9D in T-MATS provided by NASA Glenn Research Center. The operation condition of the engine model JT9D is set as follows: gas path flow $W = 639.89$ pps, enthalpy $ht = 130$ BTM/lbm, total temperature $Tt = 448.46$ degR, total pressure $Pt = 5.528$ psia and ambient pressure $Pamb = 3.626$ psia. To monitoring the engine operation, the GToMFI database is employed for training and verifying the CNN diagnosis model. The total number of the GToMFI data samples is 95375, among which 16625 samples are corresponding to the label L_0, 15750 samples are corresponding to the label L_1, 17500 samples are corresponding to the label L_2, 10500 samples are corresponding to the label L_3, 17500 samples are corresponding to the label L_4, and 17500 samples corresponding to the label L_5. 70% of these samples (66762 samples) are randomly selected as training samples, and the remaining samples (28613 samples) are used as test samples. The nature of solving the system is to use CNN to approximate the characteristics between the GToMFI data and the actuators in all fault modes, so as to realize the fault diagnosis of the turbofan engines with actuator faults. The detailed hyper-parameters of the CNN diagnosis model are shown in Table 3. The simulation platform is Python installed on a personal computer with a 64-bit Windows 10 system of Intel(R)Core(TM) i5-7400 CPU@ 3.00 GHz with 8 GB RAM.

TABLE 4. The accuracy, loss and training time of the MLP, BLSTM, and CNN diagnosis models.

Method	Training accuracy	Training loss	Testing accuracy	Testing loss	Training time
MLP	67.39%	0.7546	66.78%	0.7615	14103 s
BLSTM	86.11%	0.3582	85.97%	0.3900	246318 s
CNN	95.21%	0.1127	93.77%	0.1560	13828 s

For comparison purposes, two other diagnosis approaches, multi-layer perceptron neural network (MLP) [54] and bidirectional long short-term memory networks (BLSTM) [55] have been given. The MLP neural network adopts the structure of two hidden layers, with the learning rate 0.0001, the optimization function Adam, and the hidden layer neuron numbers 128 and 32. The BLSTM network with the learning rate of 0.0005 has three hidden layers with 16 and 16 hidden neurons in the first two hidden layers, and 128 hidden neurons in the dense layer of the third layer. The comparison of the accuracy and loss of the three methods are shown in Fig. 7. Table 4 shows the accuracy, loss, and training time of the three diagnosis models. The results of the comparison show that the accuracy of the CNN diagnosis model tends to be stable after about 100 training epochs. Although there are still some small fluctuations in the later stage, the training accuracy is

$$\begin{bmatrix} O_1(\breve{\Lambda},\breve{\Psi}) & (*) & (*) & (*) & (*) \\ O_2 & -2\gamma^2 I_{2np} & (*) & (*) & (*) \\ O_3 & 0_{2np} & -2\delta^2 I_{2np} & (*) & (*) \\ \theta\widehat{\Theta}_f(t)\Xi^T\Gamma(1,p)\breve{\Psi} & 0_{q\times 2np} & 0_{q\times 2np} & -\frac{1}{2}I_q & (*) \\ O_4\breve{\Lambda} & 0_{2np} & 0_{2np} & 0_{2np\times q} & -I_{2np} \end{bmatrix} \leq 0 \tag{43}$$

TABLE 5. Relevant parameters of the nonlinear fault-tolerant controllers.

Actuator fault Δu_f	Label	$\widehat{\phi}_f^{a,j}$ or $\widehat{\phi}_f^{m,j}$	Π	θ	γ^2	δ^2	Δu_c
$\Delta wf_f^a \in (-0.5, 0]$	L_0	$\widehat{\phi}_f^{a,1} = 0$	$0.159 I_{12}$	0.005	0.01	0	$\Delta u_c^{L_0}$
$\Delta wf_f^a \in [-0.95, -0.5]$	L_1	$\widehat{\phi}_f^{a,1} = -0.5$	$0.004 I_{12}$	0.002	0.01	0.01	$\Delta u_c^{L_1}$
$\Delta vsv_f^a \in (-0.5, 0]$	L_0	$\widehat{\phi}_f^{a,2} = 0$	$0.159 I_{12}$	0.005	0.01	0	$\Delta u_c^{L_0}$
$\Delta vsv_f^a \in (-1, -0.5]$	L_2	$\widehat{\phi}_f^{a,2} = -0.5$	$(2.512 \times 10^{-4}) I_{12}$	2.873×10^{-4}	0.01	0.01	$\Delta u_c^{L_2}$
$\Delta wf_m^f \in (-0.2, 0] \times \Delta wf_d^m$	L_0	$\widehat{\phi}_f^{m,1} = 0$	$0.159 I_{12}$	0.005	0.01	0	$\Delta u_c^{L_0}$
$\Delta wf_f^m \in (-0.5, -0.2] \times \Delta wf_m^d$	L_3	$\widehat{\phi}_f^{m,1} = -0.2$	$(2.512 \times 10^{-5}) I_{12}$	1.616×10^{-5}	0.01	0.01	$\Delta u_c^{L_3}$
$\Delta wf_f^m \in (-1, -0.5] \times \Delta wf_d^m$	L_4	$\widehat{\phi}_f^{m,1} = -0.5$	$0.999 I_{12}$	0.091	0.01	0.01	$\Delta u_c^{L_4}$
$\Delta vsv_f^m \in (-0.5, 0] \times \Delta vsv_d^m$	L_0	$\widehat{\phi}_f^{m,2} = 0$	$0.159 I_{12}$	0.0051	0.01	0	$\Delta u_c^{L_0}$
$\Delta vsv_f^m \in (-1, -0.5] \times \Delta vsv_d^m$	L_5	$\widehat{\phi}_f^{m,2} = -0.5$	$(2.512 \times 10^{-5}) I_{12}$	2.610×10^{-5}	0.01	0.01	$\Delta u_c^{L_5}$

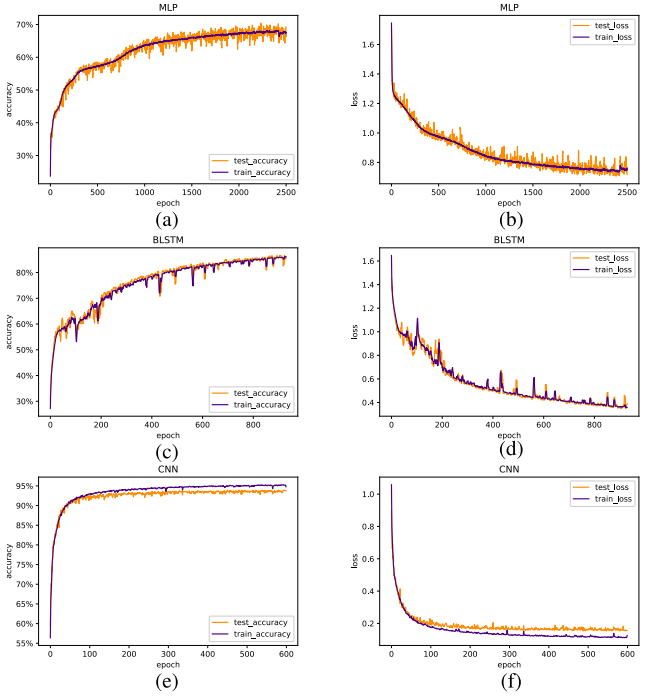

FIGURE 7. Results the accuracy and loss of MLP, BLSTM, and CNN. 7(a) Responses of the accuracy of the MLP model; 7(b) Responses of the loss of the MLP model; 7(c) Responses of the accuracy of the BLSTM model; 7(d) Responses of the loss of the BLSTM model; 7(e) Responses of the accuracy of the CNN model; 7(f) Responses of the loss of the CNN model.

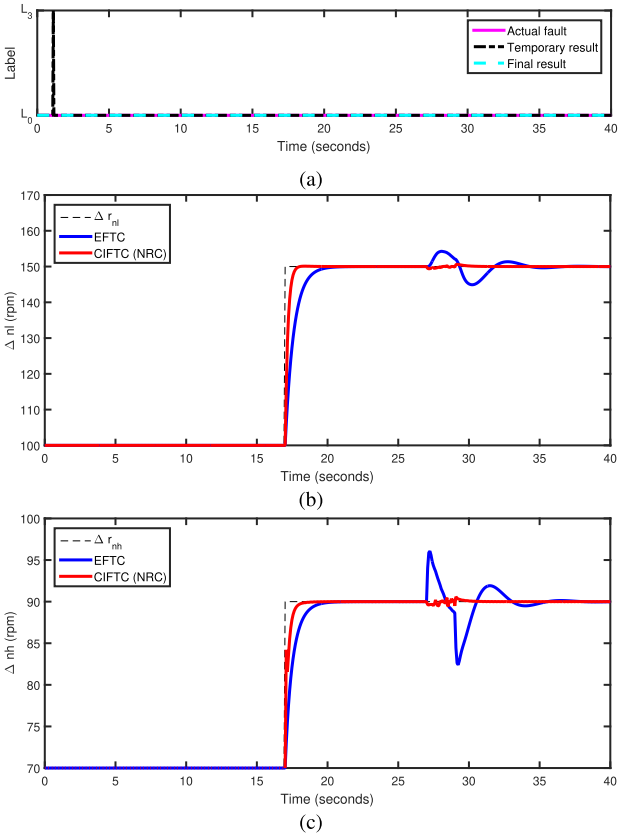

FIGURE 8. Results of the closed-loop system in fault-free case in Test 1. 8(a) Responses of the CNN-based diagnosis module; 8(b) Responses of Δnl of the JT9D engine by EFTC, NRC, and CIFTC; 8(c) Responses of Δnh of the JT9D engine by EFTC, NRC, and CIFTC. Note that the same controller $\Delta u_c^{L_0}(t)$ is adopted by NRC and CIFTC in fault-free case.

95.21% and the test accuracy approaches 93.77%. In contrast, the MLP network has the poorest diagnosis performance, and its test accuracy is as low as 66.78%. The accuracy of the BLSTM network is higher than the MLP network, but its convergence speed is slowest, and the required training epochs for convergence is much larger than CNN. In addition, the training time required for CNN is 13828 seconds, which is the shortest in the three diagnosis models. Apparently, the CNN model shows the best diagnosis performance.

Based on the CNN diagnosis model, the stack diagnosis model with $sf = 4$ gives the final fault determination (the sampling period is 0.04 seconds). In the study, the CNN-based fault diagnosis module is implemented on Python supported by TensorFlow. By using the command 'nlgreyest' of the System Identification Toolbox in MATLAB, we can obtain the normalized polynomial state-space model in (44) of the JT9D engine. Based on the engine model, the vector $\eta(t) = \left[\eta_1(t)\ \eta_2(t)\right]^T$ can be obtained in (45) by (28) without difficulty. The system matrices of the error dynamical model of the closed-loop control in (22) are given.

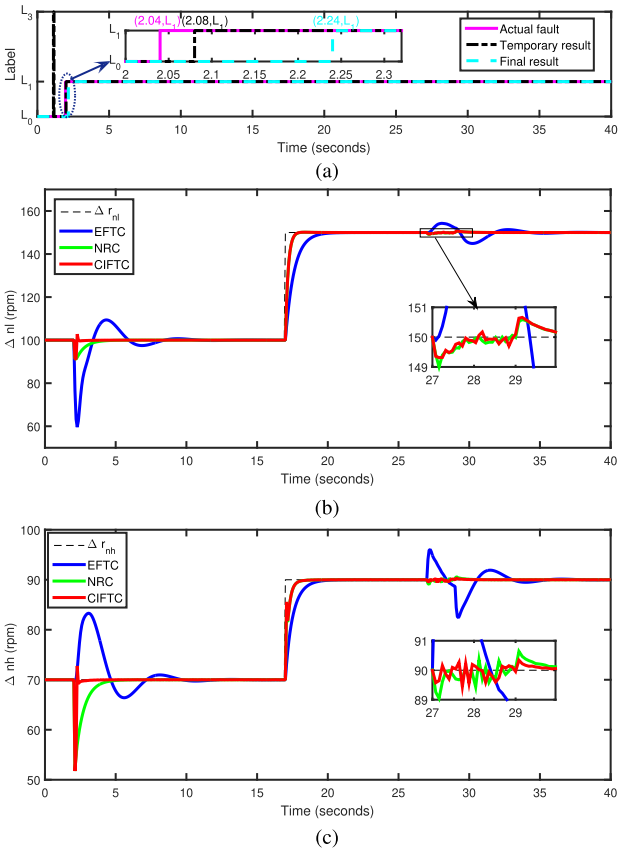

FIGURE 9. Results of the closed-loop system with $\Delta wf_f^a = 0.85$ in Test 2. 9(a) Responses of the CNN-based diagnosis module; 9(b) Responses of Δnl of the JT9D engine by EFTC, NRC, and CIFTC; 9(c) Responses of Δnh of the JT9D engine by EFTC, NRC, and CIFTC.

Hence, the nonlinear fault-tolerant controller for the JT9D engine with actuator faults are designed in (26) and (27). Choosing the relevant design parameters for actuator faults in Table 5 gives the key matrices Λ and Ψ of the nonlinear robust fault-tolerant controllers. Therefore, we can obtain the nonlinear robust fault-tolerant controllers $\Delta u_c^{L_0}(t)$-$\Delta u_c^{L_5}(t)$ in (46)−(51). For comparison purposes, the nonlinear robust controller $\Delta u_c^{L_0}(t)$ in (46) (called NRC) and the fault-tolerant controller with an estimator [56] in (52), (53), and (54) (called EFTC) are given, where $\Delta\tilde{e} = \left[\Delta\tilde{e}_{nl}\ \Delta\tilde{e}_{nh}\right]^T$ in (52) and $\Delta\tilde{u}_f = \left[\Delta\tilde{u}_{f,wf}\ \Delta\tilde{u}_{f,vsv}\right]^T$ in (53) are the estimation of the tracking errors and actuator faults of EFTC, $\Delta u_{EFTC} = \left[\Delta wf_{EFTC}\ \Delta vsv_{EFTC}\right]^T$ in (54) is the control input for the turbofan engine by EFTC.

To check the control performance for the turbofan engine, simulation is set as follows: The actuator fault event occurs at 2.04 seconds; The CNN-based fault diagnosis module monitors the operation of the turbofan engine in real-time and the corresponding nonlinear fault-tolerant controller is scheduled according to the diagnosis results and works lasted until 40 seconds; A step command is given at 17 seconds; And the pressure disturbances from Inlet and Burner ($d_1(t)$ and $d_2(t)$) are shown as follows, which helps to verify the

TABLE 6. Six tests and results with specific actuator faults.

Test	Actuator fault	Result
1	$\Delta u_f = 0$	Fig. 8
2	$\Delta wf_f^a = 0.85$	Fig. 9
3	$\Delta vsv_f^a = 0.85$	Fig. 10
4	$\Delta wf_f^m = 0.4\Delta wf_c^m$	Fig. 11
5	$\Delta wf_f^m = 0.85\Delta wf_c^m$	Fig. 12
6	$\Delta vsv_f^m = 0.85\Delta vsv_c^m$	Fig. 13

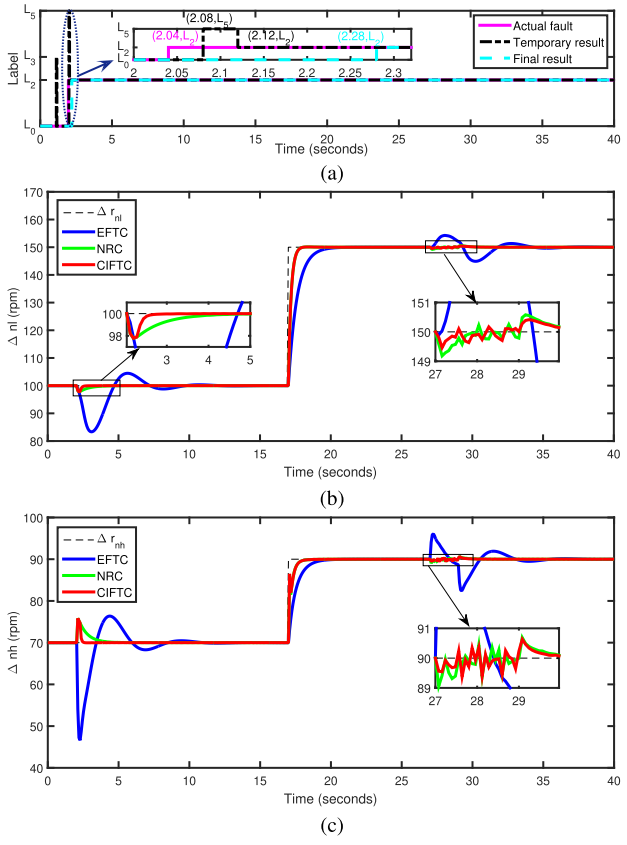

FIGURE 10. Results of the closed-loop system with $\Delta vsv_f^a = 0.85$ in Test 3. 10(a) Responses of the CNN-based diagnosis module; 10(b) Responses of Δnl of the JT9D engine by EFTC, NRC, and CIFTC; 10(c) Responses of Δnh of the JT9D engine by EFTC, NRC, and CIFTC.

disturbance rejection of the CIFTC system for turbofan engines after fault occurrence.

$$d_1(t) = \begin{cases} 0.05\big(sin(6.28t)+\mathcal{R}(0,1)\big)+0.5, & 27 \le t \le 29 \\ 0, & \text{others,} \end{cases}$$

$$d_2(t) = \begin{cases} 0.01\big(sin(62.8t)+\mathcal{R}(0,1)\big)+5, & 27 \le t \le 29 \\ 0, & \text{others,} \end{cases}$$

where $\mathcal{R}(0,1)$ denotes a random noise with zero mean and unity variance.

Six tests for the turbofan engine with some specific actuator faults are carried out as shown in Table 6. The simulation results are shown in Figs. 8−13. Moreover, the comparison of the control performance of the JT9D engine after actuator

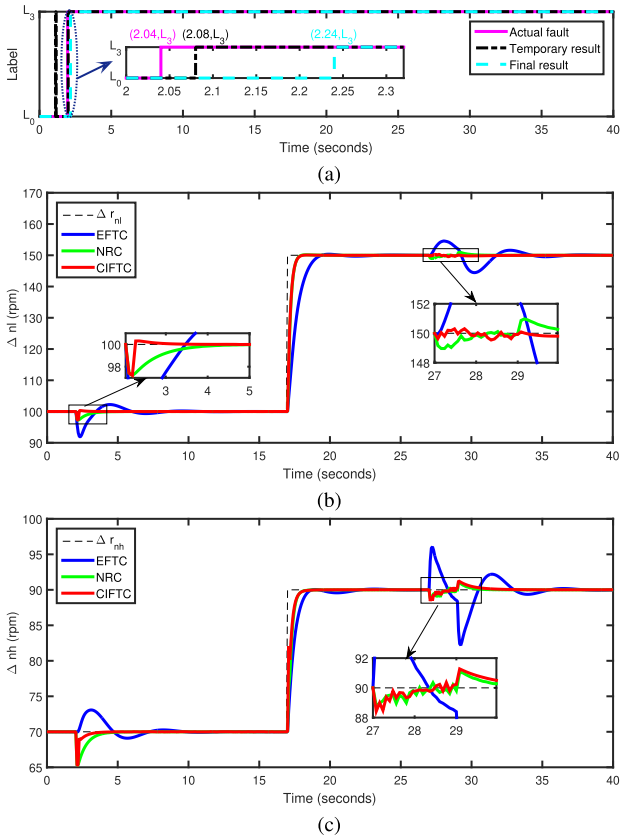

FIGURE 11. Results of the closed-loop system with $\Delta wf_f^m = 0.4\Delta wf_c^m$ in Test 4. 11(a) Responses of the CNN-based diagnosis module; 11(b) Responses of Δnl of the JT9D engine by EFTC, NRC, and CIFTC; 11(c) Responses of Δnh of the JT9D engine by EFTC, NRC, and CIFTC.

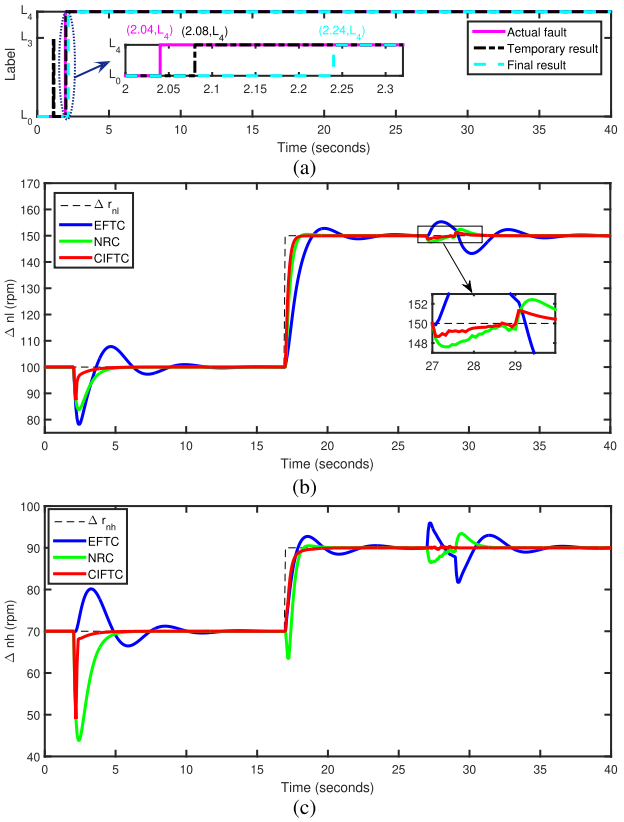

FIGURE 12. Results of the closed-loop system with $\Delta wf_f^m = 0.85\Delta wf_c^m$ in Test 5. 12(a) Responses of the CNN-based diagnosis module; 12(b) Responses of Δnl of the JT9D engine by EFTC, NRC, and CIFTC; 12(c) Responses of Δnh of the JT9D engine by EFTC, NRC, and CIFTC.

faults is shown in Fig. 14, including rise time t_r (seconds), settling time t_s (seconds), overshoot ϵ (%), the maximum value xd_{max} (rpm) and variance xd_{var} (rpm^2) of the fluctuation of the shaft speeds affected by disturbances.

According to Figs. 8−14, four observations can be generalized as follows.

1) In the case of fault-free, the states of the JT9D engine can track the reference signal by the NRC and CIFTC strategies with the same controller $\Delta u_c^{L_0}(t)$. As shown in Fig. 8, both EFTC and CIFTC (NRC) can guarantee the stable operation of the turbofan engine in the case of fault-free in Test 1. Furthermore, compared with EFTC, the proposed CIFTC strategy can help the JT9D engine complete the tracking task faster and make it less affected by disturbances.
2) Over the time interval (0, 17) of Figs. 9−13 shows that in the event of actuator faults, the states of the JT9D engine deviated from the ideal operating state instantaneously. In the occurrence of the faults, the influence of additive faults on the shaft speeds of the JT9D engine is more obvious than multiplicative faults as shown in Fig. 9 and Fig. 12. In the aspect of fault tolerance, the three control methods can all maintain the stability of the closed-loop systems even actuator faults occur. In the CIFTC system, the CNN-based fault diagnosis module can provide a reliable final diagnosis result within 0.2 seconds after the fault occurs, as shown in Figs. 9(a)−13(a). In addition, the subfigures (b) and (c) of Figs. 9−13 show that in the event of actuator faults, the shaft speeds of the JT9D engine by CIFTC can recover to the ideal state more rapidly than EFTC. Compared with NRC, the CIFTC system significantly can reduce the amplitude of fluctuation of the controlled outputs caused by the actuator faults. Thus, the proposed CIFTC system can weaken the influences of actuator faults on the JT9D engine.
3) Over the time interval (17, 27) of Figs. 9−13 shows the effects of the actuator faults on the transient performance of the JT9D engine after faults occur. The transient performance of the JT9D engine is more affected by multiplicative faults of actuators than by additive faults, as shown in Figs. 9 and 12. As shown in Figs 11−13, the CIFTC system can effectively improve the transient performance of the JT9D engine after the multiplicative faults occur. The rise time, settling time, and overshoot are important indexes to reflect the transient performance of the closed-loop system. Fig. 14 shows that the CIFTC system can improve the transient performance of the JT9D engine in the six tests. Moreover, compared

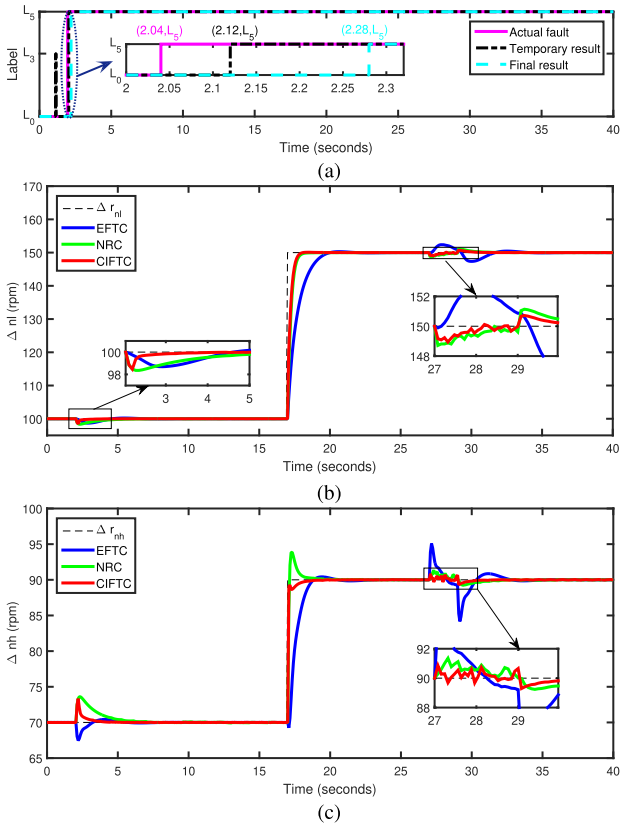

FIGURE 13. Results of the closed-loop system with $\Delta vsv_f^m = 0.85\Delta vsv_c^m$ in Test 6. 13(a) Responses of the CNN-based diagnosis module; 13(b) Responses of Δnl of the JT9D engine by EFTC, NRC, and CIFTC; 13(c) Responses of Δnh of the JT9D engine by EFTC, NRC, and CIFTC.

with EFTC, the total rise time of the CIFTC system in the six tests can be shortened by 5.87 seconds and 3.82 seconds, and the total settling time by 12.86 seconds and 13.08 seconds. Compared with NRC, the total overshoot of the speed of the high-pressure shaft by CIFTC can be reduced by 15.73%, which is beneficial to reduce the requirement of high-temperature materials and prolong the service life of turbofan engines. Hence, the CIFTC system can guarantee the transient performance of the JT9D engine after actuator faults.

4) Over the time interval (27, 40) of Figs. 9−13 shows the influence of actuator faults on the JT9D engine in terms of disturbance rejection after faults occur. Compared with NRC and EFTC, the CIFTC system can suppress the influence of external disturbances on the JT9D engine. In Fig. 12, the disturbance rejection of CIFTC is superior to EFTC and NRC significantly. The maximum value and variance value of the fluctuation caused by interference are used to reflect the ability of disturbance rejection of the closed-loop control systems. Furthermore, in Fig. 14, compared with the other two systems, the CIFTC system can keep the maximum value of the fluctuations of the controlled outputs as 8.72 rpm and 8.78 rpm, which are 84.2% and 89.0% lower than EFTC, respectively. The states controlled by CIFTC is with the smallest variance values of the fluctuation in the three closed-loop control systems, which means the proposed CIFTC can quickly restore the states at the ideal level after disturbance. Accordingly, the CIFTC system can improve the control performance of disturbance rejection for the JT9D engine after actuator faults occurrence.

VII. CONCLUSION

This paper dealt with the fault-tolerant control problem of turbofan engines with actuator faults. Aiming at actuator faults, we designed a CIFTC system for turbofan engines including the CNN-based fault diagnosis module and the nonlinear fault-tolerant controller. The CNN-based fault diagnosis module is to extract the fault information from the valuable gas-path data, which can provide fault parameters for the design of the fault-tolerant controller. According to the fault parameters, the nonlinear robust fault-tolerant controller is adjusted to ensure the stability and satisfy the L_2 gain-like performance of the closed-loop control system for turbofan engines. Simulation results are presented to illustrate the effectiveness of the proposed CIFTC strategy. Similar to other work [57], [58], the dimensionality considered in the paper is reasonable for the design of the fault-tolerant control system for turbofan engines. In future work, the proposed method will be applied for turbofan engines with higher dimensionality. Meanwhile, when the actuator fault is more complex, for example, with saturation and time-varying delay, the design

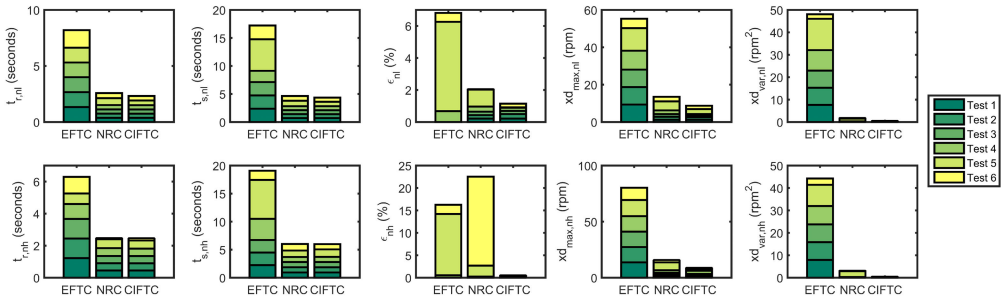

FIGURE 14. Comparison of the control performance of the JT9D engine after actuator faults occurrence by EFTC, NRC, and CITFC in Tests 1-6.

of fault-tolerant control is more challenging and the problem deserves further study. In addition, the engineering applications of the control scheme presented in this paper will form part of our further research.

APPENDIX

The polynomial state-space model of the turbofan engine is given by (44).

$$\begin{cases} \dfrac{d\Delta nl}{dt} = -2.522\Delta nl+1.094\Delta nh+0.326\Delta nl^2 \\ \quad -0.045\Delta nh^2+0.393\Delta nl^3+0.094\Delta nh^3 \\ \quad +0.851\Delta wf+0.286\Delta vsv-0.078d_1 \\ \quad -0.005d_2 \\ \dfrac{d\Delta nh}{dt} = 1.570\Delta nl-4.410\Delta nh-0.596\Delta nl^2 \\ \quad +0.035\Delta nh^2+0.124\Delta nl^3-0.063\Delta nh^3 \\ \quad +2.074\Delta wf-0.741\Delta vsv-0.202d_1 \\ \quad +0.241d_2 \end{cases} \tag{44}$$

The vector $\eta(t) = \left[\eta_1(t)\ \eta_2(t)\right]^T$ of nonlinear robust fault-tolerant controllers is given by (45).

$$\begin{cases} \eta_1(t) = -1.160\Delta nl-0.368\Delta nh+0.337\Delta nl^2 \\ \quad -0.019\Delta nh^2+0.267\Delta nl^3+0.042\Delta nh^3 \\ \quad +1.160\Delta e_{nl}+0.368\Delta e_{nh}-0.337\Delta e_{nl}^2 \\ \quad +0.019\Delta e_{nh}^2-0.267\Delta e_{nl}^3-0.042\Delta e_{nh}^3 \\ \quad -0.606\Delta\dot{r}_{nl}-0.233\Delta\dot{r}_{nh} \\ \eta_2(t) = -5.366\Delta nl+4.921\Delta nh+0.138\Delta nl^2 \\ \quad -0.101\Delta nh^2+0.580\Delta nl^3+0.203\Delta nh^3 \\ \quad +5.366\Delta e_{nl}-4.921\Delta e_{nh}-0.138\Delta e_{nl}^2 \\ \quad +0.101\Delta e_{nh}^2-0.580\Delta e_{nl}^3-0.203\Delta e_{nh}^3 \\ \quad -1.695\Delta\dot{r}_{nl}+0.695\Delta\dot{r}_{nh} \end{cases} \tag{45}$$

The nonlinear robust fault-tolerant controllers of CIFTC for the JT9D engine are given by (46)∼(51).

$$\begin{cases} \Delta wf_c^{L_0}(t) = -27.551\Delta\sigma_{nl}-9.795\Delta\sigma_{nh}-\eta_1(t) \\ \quad -16.640\Delta e_{nl}-5.817\Delta e_{nh}-0.058\Delta e_{nl}^2 \\ \quad +0.019\Delta e_{nh}^2-0.267\Delta e_{nl}^3-0.043\Delta e_{nh}^3 \\ \Delta vsv_c^{L_0}(t) = -73.332\Delta\sigma_{nl}+33.848\Delta\sigma_{nh}-\eta_2(t) \\ \quad -42.193\Delta e_{nl}+17.055\Delta e_{nh}-0.967\Delta e_{nl}^2 \\ \quad +0.100\Delta e_{nh}^2-0.580\Delta e_{nl}^3-0.204\Delta e_{nh}^3 \end{cases} \tag{46}$$

$$\begin{cases} \Delta wf_c^{L_1}(t) = -28.333\Delta\sigma_{nl}-16.962\Delta\sigma_{nh}-\eta_1(t) \\ \quad -17.118\Delta e_{nl}-9.712\Delta e_{nh}-0.060\Delta e_{nl}^2 \\ \quad +0.019\Delta e_{nh}^2-0.269\Delta e_{nl}^3-0.043\Delta e_{nh}^3 \\ \quad +0.5 \\ \Delta vsv_c^{L_1}(t) = -63.855\Delta\sigma_{nl}+31.012\Delta\sigma_{nh}-\eta_2(t) \\ \quad -37.181\Delta e_{nl}+15.477\Delta e_{nh}-0.974\Delta e_{nl}^2 \\ \quad +0.101\Delta e_{nh}^2-0.585\Delta e_{nl}^3-0.205\Delta e_{nh}^3 \end{cases} \tag{47}$$

$$\begin{cases} \Delta wf_c^{L_2}(t) = -33.264\Delta\sigma_{nl}-13.980\Delta\sigma_{nh}-\eta_1(t) \\ \quad -19.636\Delta e_{nl}-7.991\Delta e_{nh}-0.058\Delta e_{nl}^2 \\ \quad +0.019\Delta e_{nh}^2-0.267\Delta e_{nl}^3-0.043\Delta e_{nh}^3 \\ \Delta vsv_c^{L_2}(t) = -86.155\Delta\sigma_{nl}+39.192\Delta\sigma_{nh}-\eta_2(t) \\ \quad -49.071\Delta e_{nl}+19.750\Delta e_{nh}-0.967\Delta e_{nl}^2 \\ \quad +0.100\Delta e_{nh}^2-0.580\Delta e_{nl}^3-0.204\Delta e_{nh}^3 \\ \quad +0.5 \end{cases} \tag{48}$$

$$\begin{cases} \Delta wf_c^{L_3}(t) = -49.173\Delta\sigma_{nl}-17.360\Delta\sigma_{nh}-1.25\eta_1(t) \\ \quad -28.591\Delta e_{nl}-10.109\Delta e_{nh}-0.073\Delta e_{nl}^2 \\ \quad +0.024\Delta e_{nh}^2-0.333\Delta e_{nl}^3-0.053\Delta e_{nh}^3 \\ \Delta vsv_c^{L_3}(t) = -107.282\Delta\sigma_{nl}+47.882\Delta\sigma_{nh}-\eta_2(t) \\ \quad -60.165\Delta e_{nl}+24.372\Delta e_{nh}-0.966\Delta e_{nl}^2 \\ \quad +0.100\Delta e_{nh}^2-0.579\Delta e_{nl}^3-0.204\Delta e_{nh}^3 \end{cases} \tag{49}$$

$$\begin{cases} \Delta wf_c^{L_4}(t) = -107.421\Delta\sigma_{nl}-16.386\Delta\sigma_{nh}-2\eta_1(t) \\ \quad -77.601\Delta e_{nl}-30.362\Delta e_{nh}-14.779\Delta e_{nl}^2 \\ \quad +2.698\Delta e_{nh}^2-29.485\Delta e_{nl}^3-5.807\Delta e_{nh}^3 \\ \Delta vsv_c^{L_4}(t) = -25.322\Delta\sigma_{nl}+16.342\Delta\sigma_{nh}-\eta_2(t) \\ \quad -16.435\Delta e_{nl}+7.024\Delta e_{nh}-4.113\Delta e_{nl}^2 \\ \quad +0.689\Delta e_{nh}^2-7.104\Delta e_{nl}^3-1.472\Delta e_{nh}^3 \end{cases} \tag{50}$$

$$\begin{cases} \Delta wf_c^{L_5}(t) = -42.181\Delta\sigma_{nl}-15.784\Delta\sigma_{nh}-\eta_1(t) \\ \quad -24.559\Delta e_{nl}-9.045\Delta e_{nh}-0.058\Delta e_{nl}^2 \\ \quad +0.019\Delta e_{nh}^2-0.267\Delta e_{nl}^3-0.043\Delta e_{nh}^3 \\ \Delta vsv_c^{L_5}(t) = -226.099\Delta\sigma_{nl}+100.769\Delta\sigma_{nh}-2\eta_2(t) \\ \quad -127.731\Delta e_{nl}+51.907\Delta e_{nh}-1.932\Delta e_{nl}^2 \\ \quad +0.201\Delta e_{nh}^2-1.158\Delta e_{nl}^3-0.407\Delta e_{nh}^3 \end{cases} \tag{51}$$

The estimator of EFTC for the JT9D engine is given by (52) and (53).

$$\begin{cases} \Delta\dot{\tilde{e}}_{nl}(t) = -2.522\Delta\tilde{e}_{nl}+1.094\Delta\tilde{e}_{nh}+0.326\Delta\tilde{e}_{nl}^2 \\ \quad -0.045\Delta\tilde{e}_{nh}^2+0.393\Delta\tilde{e}_{nl}^3-0.094\Delta\tilde{e}_{nh}^3 \\ \quad +0.851\Delta wf_{EFTC}(t)+0.286\Delta vsv_{EFTC}(t) \\ \quad +0.851\Delta\tilde{u}_{wf,f}(t)+0.286\Delta\tilde{u}_{vsv,f}(t) \\ \quad +6.478(\Delta e_{nl}-\Delta\tilde{e}_{nl})+1.094(\Delta e_{nh}-\Delta\tilde{e}_{nh}) \\ \Delta\dot{\tilde{e}}_{nh}(t) = 1.570\Delta\tilde{e}_{nl}-4.410\Delta\tilde{e}_{nh}-0.596\Delta\tilde{e}_{nl}^2 \\ \quad +0.035\Delta\tilde{e}_{nh}^2+0.124\Delta\tilde{e}_{nl}^3-0.063\Delta\tilde{e}_{nh}^3 \\ \quad +2.074\Delta wf_{EFTC}(t)-0.741\Delta vsv_{EFTC}(t) \\ \quad +2.074\Delta\tilde{u}_{wf,f}(t)-0.741\Delta\tilde{u}_{vsv,f}(t) \\ \quad +1.570(\Delta e_{nl}-\Delta\tilde{e}_{nl})+10.590(\Delta e_{nh}-\Delta\tilde{e}_{nh}) \end{cases} \tag{52}$$

$$\begin{cases} \Delta\dot{\tilde{u}}_{wf,f}(t) = 74.817(\Delta e_{nl}-\Delta\tilde{e}_{nl}) \\ \quad +12.636(\Delta e_{nh}-\Delta\tilde{e}_{nh}) \\ \Delta\dot{\tilde{u}}_{vsv,f}(t) = 18.134(\Delta e_{nl}-\Delta\tilde{e}_{nl}) \\ \quad +122.312(\Delta e_{nh}-\Delta\tilde{e}_{nh}) \end{cases} \tag{53}$$

The nonlinear fault-tolerant controller of EFTC for the JT9D engine is given by (52).

$$\begin{cases} \Delta wf_{EFTC}(t) = 0.569\Delta\tilde{e}_{nl}+0.998\Delta\tilde{e}_{nh}-0.058\Delta\tilde{e}_{nl}^2 \\ \quad +0.019\Delta\tilde{e}_{nh}^2-0.267\Delta\tilde{e}_{nl}^3+0.043\Delta\tilde{e}_{nh}^3 \\ \quad -0.606\Delta\tilde{u}_{wf,f}(t)-0.234\Delta\tilde{u}_{vsv,f}(t) \\ \Delta vsv_{EFTC}(t) = 5.372\Delta\tilde{e}_{nl}-2.482\Delta\tilde{e}_{nh}-0.966\Delta\tilde{e}_{nl}^2 \\ \quad +0.100\Delta\tilde{e}_{nh}^2-0.579\Delta\tilde{e}_{nl}^3-0.204\Delta\tilde{e}_{nh}^3 \\ \quad -1.694\Delta\tilde{u}_{wf,f}(t)+0.695\Delta\tilde{u}_{vsv,f}(t) \end{cases} \tag{54}$$

ACKNOWLEDGMENT

(Dingding Cheng and Lijun Liu are co-first authors.)

REFERENCES

[1] W. Chen, F. N. Chowdhury, A. Djuric, and C.-P. Yeh, "Robust fault detection of turbofan engines subject to adaptive controllers via a total measurable fault information residual (ToMFIR) technique," *ISA Trans.*, vol. 53, no. 5, pp. 1383–1388, Sep. 2014.

[2] E. Naderi and K. Khorasani, "Data-driven fault detection, isolation and estimation of aircraft gas turbine engine actuator and sensors," *Mech. Syst. Signal Process.*, vol. 100, pp. 415–438, Feb. 2018.

[3] N. Meskin, E. Naderi, and K. Khorasani, "A multiple model-based approach for fault diagnosis of jet engines," *IEEE Trans. Control Syst. Technol.*, vol. 21, no. 1, pp. 254–262, Jan. 2013.

[4] X. Zhang, L. Tang, and J. Decastro, "Robust fault diagnosis of aircraft engines: A nonlinear adaptive estimation-based approach," *IEEE Trans. Control Syst. Technol.*, vol. 21, no. 3, pp. 861–868, May 2013.

[5] L. Shang and G. Liu, "Sensor and actuator fault detection and isolation for a high performance aircraft engine bleed air temperature control system," *IEEE Trans. Control Syst. Technol.*, vol. 19, no. 5, pp. 1260–1268, Sep. 2011.

[6] R. Loureiro, S. Benmoussa, Y. Touati, R. Merzouki, and B. O. Bouamama, "Integration of fault diagnosis and fault-tolerant control for health monitoring of a class of MIMO intelligent autonomous vehicles," *IEEE Trans. Veh. Technol.*, vol. 63, no. 1, pp. 30–39, Jan. 2014.

[7] Q. Shen, B. Jiang, P. Shi, and C.-C. Lim, "Novel neural networks-based fault tolerant control scheme with fault alarm," *IEEE Trans. Cybern.*, vol. 44, no. 11, pp. 2190–2201, Nov. 2014.

[8] X. Yang, L. Gou, and Q. Shen, "Research of aero-engine robust fault-tolerant control based on linear matrix inequality approach," in *Electronics and Signal Processing* (Lecture Notes in Computer Science). Berlin, Germany: Springer, 2011, pp. 315–323.

[9] A. A. Amin and K. M. Hasan, "A review of fault tolerant control systems: Advancements and applications," *Measurement*, vol. 143, pp. 58–68, Sep. 2019.

[10] M. Tayyeb, U. Riaz, A. A. Amin, O. Saleem, M. Arslan, and M. H. Shahbaz, "Design of highly redundant fault tolerant control for aircraft elevator system," *J. Appl. Eng. Sci.*, pp. 1–11, Nov. 2020, doi: 10.5937/jaes0-27611.

[11] S. Ahmed, A. A. Amin, Z. Wajid, and F. Ahmad, "Reliable speed control of a permanent magnet DC motor using fault-tolerant H-bridge," *Adv. Mech. Eng.*, vol. 12, no. 10, pp. 1–14, Oct. 2020.

[12] A. A. Amin and K. Mahmood-ul-Hasan, "Hybrid fault tolerant control for air–fuel ratio control of internal combustion gasoline engine using Kalman filters with advanced redundancy," *Meas. Control*, vol. 52, nos. 5–6, pp. 473–492, Jun. 2019.

[13] A. A. Amin and K. Mahmood-Ul-Hasan, "Advanced fault tolerant air-fuel ratio control of internal combustion gas engine for sensor and actuator faults," *IEEE Access*, vol. 7, pp. 17634–17643, Feb. 2019.

[14] P. Gutiérrez-León, J. García-Morales, R. F. Escobar-Jiménez, J. F. Gómez-Aguilar, G. López-López, and L. Torres, "Implementation of a fault tolerant system for the internal combustion engine's MAF sensor," *Measurement*, vol. 122, pp. 91–99, Jul. 2018.

[15] A. A. Amin and K. Mahmood-ul-Hasan, "Robust active fault-tolerant control for internal combustion gas engine for air–fuel ratio control with statistical regression-based observer model," *Meas. Control*, vol. 52, nos. 9–10, pp. 1179–1194, Nov. 2019.

[16] Y. Yuan, X. Liu, S. Ding, and B. Pan, "Fault detection and location system for diagnosis of multiple faults in aeroengines," *IEEE Access*, vol. 5, pp. 17671–17677, Aug. 2017.

[17] K. Takahisa and D. L. Simon, "Aircraft engine sensor/actuator/component fault diagnosis using a bank of Kalman filters," NASA/CR, Cleveland, OH, USA, Tech. Rep. NASA/CR-2003-212298, May 2003.

[18] K. Takahisa and D. L. Simon, "Hybrid Kalman filter: A new approach for aircraft engine in-flight diagnostics," NASA/CR, Cleveland, OH, USA, Tech. Rep. NASA/CR-2003-212298, Dec. 2006.

[19] P. Zhang and J. Q. Huang, "Aeroengine fault diagnosis using dual Kalman filtering technique," *J. Aerosp. Power*, vol. 23, no. 5, pp. 952–956, May 2008.

[20] F. Lu, J. Huang, and Y. Lv, "Gas path health monitoring for a turbofan engine based on a nonlinear filtering approach," *Energies*, vol. 6, no. 1, pp. 492–513, Jan. 2013.

[21] X. Zhou, F. Lu, and J. Huang, "Fault diagnosis based on measurement reconstruction of HPT exit pressure for turbofan engine," *Chin. J. Aeronaut.*, vol. 32, no. 5, pp. 1156–1170, May 2019.

[22] L. Gou, L. Wang, Z. Zhou, A. Liang, and Z. Liu, "Fault diagnosis for actuator of aero-engine based on associated observers," in *Proc. Chin. Control Conf.*, 2018, pp. 6110–6114.

[23] Y. Jin and W. Chen, "Robust fault detection and estimation for turbofan engines subject to adaptive controllers via observer and ToMFIR techniques," in *Proc. 9th IEEE Conf. Ind. Electron. Appl.*, Jun. 2014, pp. 672–677.

[24] D. Simon and D. L. Simon, "Constrained Kalman filtering via density function truncation for turbofan engine health estimation," *Int. J. Syst. Sci.*, vol. 41, no. 2, pp. 159–171, Feb. 2010.

[25] X. Chang, J. Huang, F. Lu, and H. Sun, "Gas-path health estimation for an aircraft engine based on a sliding mode observer," *Energies*, vol. 9, no. 8, pp. 1–15, Jul. 2016.

[26] X. Chang, J. Huang, and F. Lu, "Health parameter estimation with second-order sliding mode observer for a turbofan engine," *Energies*, vol. 10, no. 7, pp. 1–19, Jul. 2017.

[27] Y. Yuan, S. Ding, X. Liu, and Q. Pan, "Hybrid diagnosis system for aeroengine sensor and actuator faults," *J. Aerosp. Eng.*, vol. 33, no. 1, pp. 1–11, Apr. 2020.

[28] M. Moghaddam, Q. Chen, and A. V. Deshmukh, "A neuro-inspired computational model for adaptive fault diagnosis," *Expert Syst. Appl.*, vol. 14, no. 112879, pp. 1–11, Aug. 2019.

[29] D. Yang, G. Zong, and J. Zhao, "H_∞ fault-tolerant control for switched linear parameter-varying systems: A parameter and state-dependent switching method with dwell time," *Proc. IMechE I, J. Syst. Control Eng.*, vol. 233, no. 1, pp. 18–30, Apr. 2018.

[30] U. Riaz, M. Tayyeb, and A. A. Amin, "A review of sliding mode control with the perspective of utilization in fault tolerant control," *Recent Adv. Electr. Electron. Eng. (Formerly Recent Patents Electr. Electron. Eng.)*, vol. 13, pp. 1–16, Nov. 2020.

[31] R. Sakthivel, M. Joby, C. Wang, and B. Kaviarasan, "Finite-time fault-tolerant control of neutral systems against actuator saturation and nonlinear actuator faults," *Appl. Math. Comput.*, vol. 332, pp. 425–436, Sep. 2018.

[32] B. Kaviarasan, R. Sakthivel, and O. M. Kwon, "Robust fault-tolerant control for power systems against mixed actuator failures," *Nonlinear Anal. Hybrid Syst.*, vol. 22, pp. 249–261, Nov. 2016.

[33] J. Jiang and X. Yu, "Fault-tolerant control systems: A comparative study between active and passive approaches," *Annu. Rev. Control*, vol. 36, no. 1, pp. 60–72, Apr. 2012.

[34] X. Liu, Z. Gao, and A. Zhang, "Robust fault tolerant control for discrete-time dynamic systems with applications to aero engineering systems," *IEEE Access*, vol. 6, pp. 18832–18847, Mar. 2018.

[35] L. Xiao, Y. Du, J. Hu, and B. Jiang, "Sliding mode fault tolerant control with adaptive diagnosis for aircraft engines," *Int. J. Turbo Jet-Engines*, vol. 35, no. 1, pp. 49–57, Mar. 2018.

[36] X. Chang, J. Huang, and F. Lu, "Sensor fault tolerant control for aircraft engines using sliding mode observer," *Energies*, vol. 12, no. 21, p. 4109, Oct. 2019.

[37] J. Xu, X. Liu, B. Wang, and J. Lin, "Deep belief network-based gas path fault diagnosis for turbofan engines," *IEEE Access*, vol. 7, pp. 170333–170342, Nov. 2019.

[38] R. Wang, M. Liu, and Y. Ma, "Fault estimation for aeroengine LPV systems based on LFT," *Asian J. Control*, pp. 1–11, Jun. 2019.

[39] D. Feng, M. Xiao, Y. Liu, H. Song, Z. Yang, and L. Zhang, "A kernel principal component analysis–based degradation model and remaining useful life estimation for the turbofan engine," *Adv. Mech. Eng.*, vol. 8, no. 5, pp. 1–13, Apr. 2016.
[40] M. T. Yildirim and B. Kurt, "Aircraft gas turbine engine health monitoring system by real flight data," *Int. J. Aerosp. Eng.*, vol. 2018, pp. 1–12, Mar. 2018.
[41] M. Yuan, Y. Wu, and L. Lin, "Fault diagnosis and remaining useful life estimation of aero engine using LSTM neural network," in *Proc. IEEE/CSAA Int. Conf. Aircr. Utility Syst.*, Oct. 2016, pp. 135–140.
[42] R. B. Joly, S. O. T. Ogaji, R. Singh, and S. D. Probert, "Gas-turbine diagnostics using artificial neural-networks for a high bypass ratio military turbofan engine," *Appl. Energy*, vol. 78, no. 4, pp. 397–418, Aug. 2004.
[43] J. Gu, Z. Wang, J. Kuen, L. Ma, A. Shahroudy, B. Shuai, T. Liu, X. Wang, G. Wang, J. Cai, and T. Chen, "Recent advances in convolutional neural networks," *Pattern Recognit.*, vol. 77, no. 2018, pp. 354–377, Oct. 2017.
[44] F. Karim, S. Majumdar, H. Darabi, and S. Chen, "LSTM fully convolutional networks for time series classification," *IEEE Access*, vol. 6, pp. 1662–1669, Nov. 2018.
[45] J. H. Lee, J. H. Pack, and I. S. Lee, "Fault diagnosis of induction motor using convolutional neural network," *Appl. Sci.*, vol. 9, no. 2950, pp. 1–10, Jul. 2019.
[46] Y. Ma, X. Jia, H. Bai, G. Liu, G. Wang, C. Guo, and S. Wang, "A new fault diagnosis method based on convolutional neural network and compressive sensing," *J. Mech. Sci. Technol.*, vol. 33, no. 11, pp. 5177–5188, Nov. 2019.
[47] W. Gong, H. Chen, Z. Zhang, M. Zhang, and H. Gao, "A data-driven-based fault diagnosis approach for electrical power DC-DC inverter by using modified convolutional neural network with global average pooling and 2-D feature image," *IEEE Access*, vol. 8, pp. 73677–73697, Apr. 2020.
[48] T. Han, C. Liu, W. Yang, and D. Jiang, "A novel adversarial learning framework in deep convolutional neural network for intelligent diagnosis of mechanical faults," *Knowl.-Based Syst.*, vol. 165, pp. 474–487, Feb. 2019.
[49] N. Ouyang, T. Zhu, and L. Lin, "Convolutional neural network trained by joint loss for hyperspectral image classification," *IEEE Geosci. Remote Sens. Lett.*, vol. 16, no. 3, pp. 457–461, Mar. 2019.
[50] W. Sun, R. Zhao, R. Yan, S. Shao, and X. Chen, "Convolutional discriminative feature learning for induction motor fault diagnosis," *IEEE Trans. Ind. Informat.*, vol. 13, no. 3, pp. 1350–1359, Jun. 2017.
[51] W. Gong, H. Chen, Z. Zhang, M. Zhang, R. Wang, C. Guan, and Q. Wang, "A novel deep learning method for intelligent fault diagnosis of rotating machinery based on improved CNN-SVM and multichannel data fusion," *Sensors*, vol. 19, no. 1693, pp. 1–37, Apr. 2019.
[52] D. P. Kingma and J. Ba, "Adam: A method for stochastic optimization," 2014, *arXiv:1412.6980*. [Online]. Available: http://arxiv.org/abs/1412.6980
[53] S. Ioffe and C. Szegedy, "Batch normalization: Accelerating deep network training by reducing internal covariate shift," in *Proc. Int. Conf. Mach. Learn.*, Jul. 2015, pp. 448–456.
[54] D. Chen and W. J. Wang, "Classification of wavelet map patterns using multi-layer neural networks for gear fault detection," *Mech. Syst. Signal Process.*, vol. 16, no. 4, pp. 695–704, Mar. 2002.
[55] C.-G. Huang, H.-Z. Huang, and Y.-F. Li, "A bidirectional LSTM prognostics method under multiple operational conditions," *IEEE Trans. Ind. Electron.*, vol. 66, no. 11, pp. 8792–8802, Nov. 2019.
[56] L. Ma, Y. Huang, L. Zhou, J. Wang, and D. Shi, "Fault tolerant control for a class of nonlinear system with actuator faults," *Asian J. Control*, vol. 2019, pp. 1–12, Sep. 2019.
[57] H. Richter, *Advanced Control of Turbofan Engines*. New York, NY, USA: Springer, 2012.
[58] J. Wang, G. Dimirovski, and H. Yue, "Finite-time regulation of two-spool turbofan engines with one shaft speed control," *J. Dyn. Syst., Meas., Control*, vol. 138, no. 8, pp. 1–7, Aug. 2016.

DINGDING CHENG received the B.S. degree in electrical engineering and automation and the M.S. degree in control science and engineering from the Hebei University of Science and Technology, Shijiazhuang, China, in 2014 and 2017, respectively. She is currently pursuing the Ph.D. degree with the School of Aerospace Engineering, Xiamen University, China. Her current research interests include nonlinear robust control, fault diagnosis, and fault tolerant control.

LIJUN LIU received the B.S. degree in mathematics from Jilin University, in 2007, and the M.E. and Ph.D. degrees in control science and engineering from the Harbin Institute of Technology, in 2009 and 2013, respectively. From 2009 to 2011, he was a Visiting Scholar with Duke University. From 2017 to 2020, he was a Postdoctoral Researcher with the Research and Development Center, AECC Commercial Aircraft Engine Company Ltd. He is currently an Associate Professor with the School of Aerospace Engineering, Xiamen University. His research interests include nonlinear control, aeroengine control, fault diagnosis and fault-tolerant control, and computational electromagnetics.

ZHEN YU received the B.S. and M.S. degrees from Harbin Engineering University, in 1985 and 1988, respectively, and the Ph.D. degree from Xiamen University, in 2009. Since 2009, he has been a Professor with the Department of Automation, Xiamen University. From 2014 to 2015, he was a Visiting Scholar with Louisiana State University. His research interests include control engineering, fault diagnosis, and fault-tolerant control.